sussreport+

THE CUSTOMER MAGAZINE OF SUSS MICROTEC | ISSUE 2017

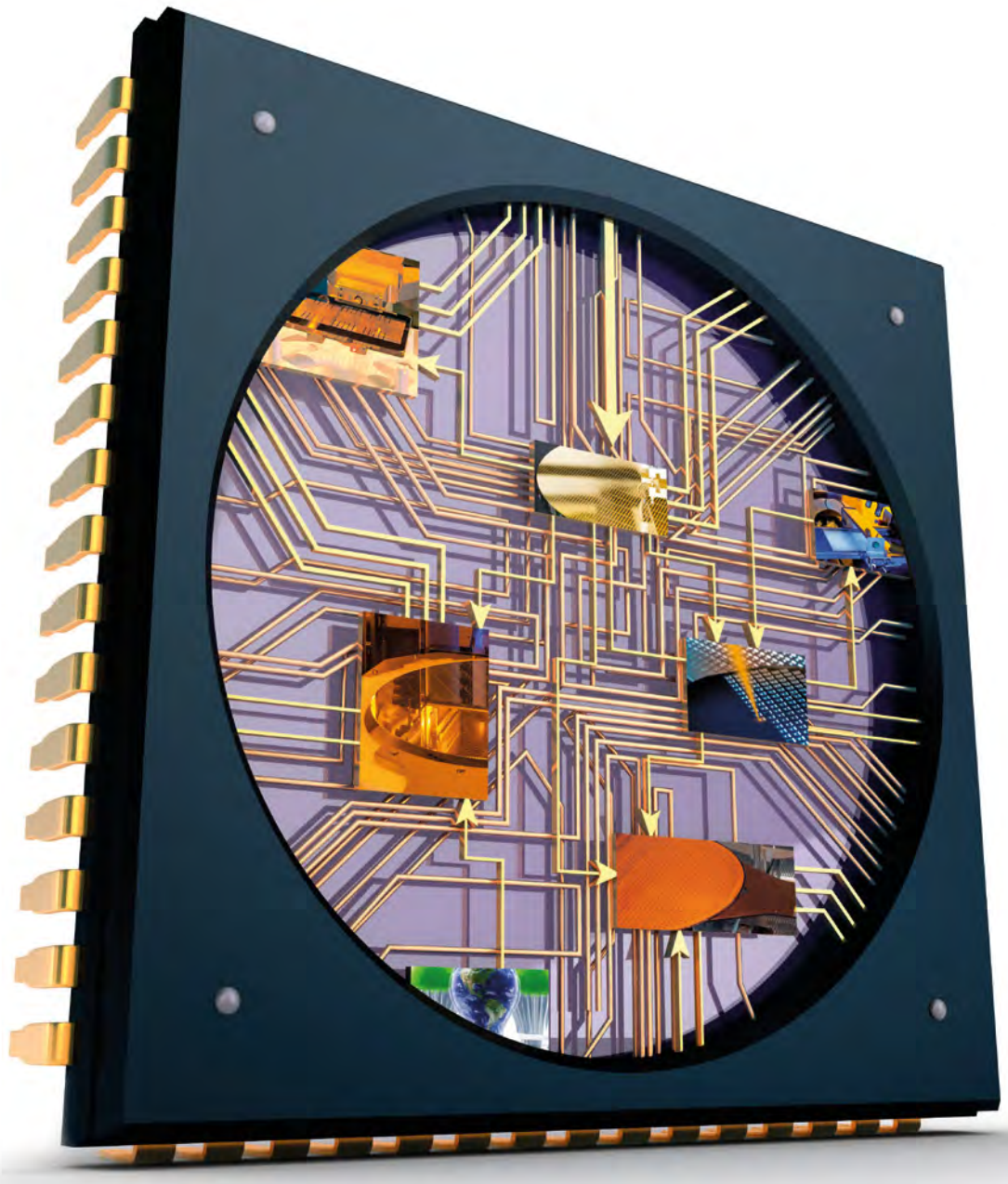

SÜSS MicroTec

+ INDEX

EDITORIAL

IN THE SPOTLIGHT

+ EDITORIAL

Dr. Franz Richter, CEO, SÜSS MicroTec SE

Dear Reader,

The semiconductor industry's outlook for the next year is quite positive. Analysts forecast growth rates of approximately 20 % worldwide for the year 2018. As SUSS MicroTec plays a strong role in many segments of the semiconductor market, we will benefit from this growth. We work in close collaboration with the main players in the industry and develop equipment tailored to their needs. Our very demanding customers rely on the high performance and known reliability of SUSS equipment. They know that they will only meet the stringent requirements of their markets with reliable, high quality equipment. And this is, what we strive for.

To help our customer succeed in future, we heavily engage in the development of new technologies. We provide important new enhancements for the MEMS and Advanced Packaging markets, targeting special packaging technologies such as 2.5D and 3D integration, interposers and fan-out wafer-level packaging. A focus has been on SUSS MicroTec's proprietary 1x full-field projection scanner technology. A novel optical magnification correction will significantly improve overlay accuracy – a feature that will provide valuable advantages especially for FOWLP applications. With its higher throughput capabilities and lower cost of ownership our scanner technology proves once more to be superior in competitiveness compared to standard stepper technology.

We have complemented our proven XB bond platform with another highlight, a novel laser pre-bond process to improve post-bond alignment accuracy. This technology will come in handy for a wide variety of MEMS applications.

Supporting growth rates also calls for consideration for the environment. This encompasses dealing with resources in a responsible way as well as developing sustainable technologies. Often enough protection of the environment, however, means extra costs. We are therefore quite proud that with the new LED lamp house for our mask aligners we succeeded in coming up with environmentally-friendly technology and lower cost of ownership at the same time. A study has been conducted to analyze the ecological footprint of our LED technology.

We at SUSS MicroTec help our customers to secure an important advantage by supplying innovative solutions. But we are not alone – a strong network of partners is supporting us. We work with research institutes and partners in industry to be able to offer a complete solution – specially designed for individual needs. All parties engage in continuously improving performance and efficiency. The recent findings about the SCIL technology that will facilitate future industrial applications serve as an example for such a successful partnership.

And last but not least, it is our customers that help us to stay at the forefront of innovation. With their expertise and input we are able to continuously excel ourselves.

Enjoy reading the SUSS Report 2017 !

Franz Richter

OPTICAL MAGNIFICATION CORRECTION APPLIED TO FULL-FIELD 1X PROJECTION LITHOGRAPHY FOR FAN-OUT

Matthew Gingerella and Markus Arendt SUSS MicroTec Photonic Systems Inc., Corona, USA

This paper describes a *new Optical Magnification-Correction* and Beam-Steering technology to improve full-field lithography overlay for fan-out wafers by actively mitigating magnification (mag) errors – wafer to wafer. This technology is targeted to enable correction for up to ± 200 ppm symmetric mag and ± 50 ppm of asymmetric mag. The patent pending mag compensation function includes a zoom lens and a dual gimbal beam-steering assembly, both with closed loop feedback, integrated into the SUSS DSC300 Gen3 projection scanner platform (available Q2/2018). Preliminary proof-of-concept test data *for the proprietary beam-steering control are reported and discussed.*

Mask-less laser direct imaging (LDI) technologies, or die-by-die alignment strategies on steppers can deal with these error contributions, but they cannot provide adequate throughput and have a high cost-of-ownership, and therefore offer a limited solution for the industry.

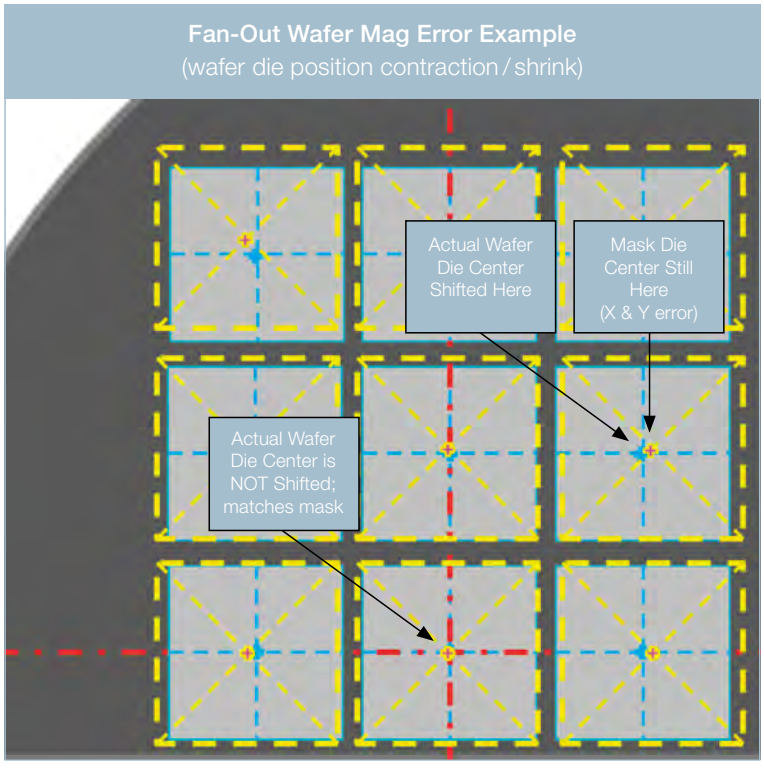

Figure 1 *Illustration of fan-out wafer die and mask pattern mismatch due to magnification error*

INTRODUCTION

Today's requirements for finer features in advanced Wafer-Level Packaging (WLP) applications create the additional need for tighter overlay control from lithography equipment. The improvement goes beyond the inherent overlay capability of the equipment ("tool-to-itself"), and requires ways to actively compensate for mismatches in actual feature size and position on the wafer with respect to the photomask pattern (Figure 1).

Controlling a good overlay accuracy is especially challenging when using Fan-out Wafer Level Packaging (FO-WLP). Here, the dies are embedded in an artificial reconstituted wafer made of epoxy mold compound (EMC), and the resulting overlay sees a stack-up of "random errors" and "systematic errors". The random contribution is mostly a result of the accuracy of the die placement equipment, and can be controlled to errors in the range of 2 µm to 5 µm, depending on the quality and speed of the selected system. The dominant systematic error term to correct for is a magnification error [1] that is mainly caused by thermal compression molding and curing of the EMC. The mag induced die shifts easily reach and exceed 100-200 ppm [2], or 15-30 µm on a 300 mm wafer, so correcting for the systematic error can be a good alignment methodology [1].

An efficient way to compensate for the high systematic error is provided by the proposed magnification correction technology. The implementation of mag correction technology in the SUSS DSC300 Gen3 projection scanner platform (Figure 2) enables the full correction of magnification errors up to ± 200 ppm in X and Y (symmetric) and ± 50 ppm in X or Y (asymmetric) at high throughput and with no stitching.

Figure 2 SUSS DSC300 Projection Scanner

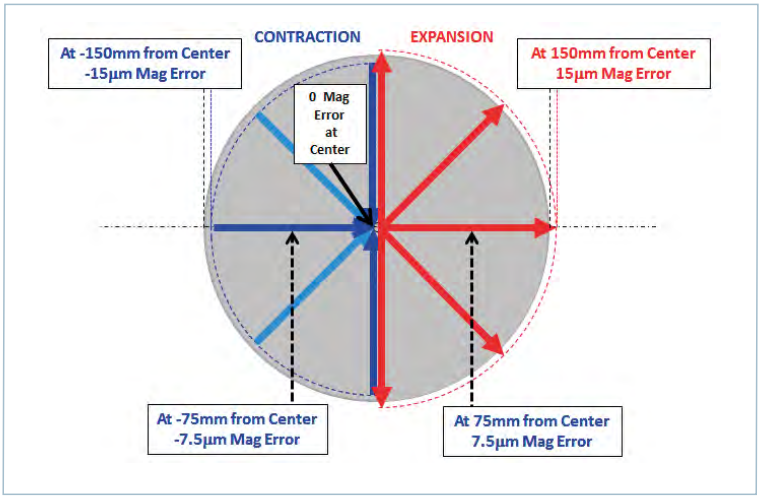

Figure 3 Mag errors as a function of distance from wafer center

Along with the magnification correction technology, Fan-Out applications can make use of all benefits of the DSC300 full-field projection technology:

- Non-repeated features like different dies and packages, for example for heterogeneous integration
- Invariant to package sizes: even very large packages can be processed without stitching
- No need for edge protection and edge exposure
- No throughput impact through adjustment of exposure window to package sizes
- Highest throughput among all advanced lithography systems through continuous exposure, with no throughput loss through optical magnification

IMPACT OF MAG ERRORS ON OVERLAY

Large amounts of uncorrected magnification error can significantly diminish overlay accuracy Since the amount of mag error is dependent on the specific distance from the center of the wafer (at center magnification error is zero), 300 mm diameter wafer processing has the potential for larger absolute overlay errors than 200 mm diameter wafers. As shown in Figure 3, at a distance of 75 mm from the center of a 300 mm diameter wafer with 100 ppm (parts per million) of magnification (expansion or contraction), the absolute mag error is 7.5 µm. At 150 mm from center, the absolute mag error is already 15 µm (2X since it is a linear function); per equations 1-3.

Mag Error Equations (1-3)

Eq. 1: Convert PPM to Ratio (R_{mag}):
ppm = N parts / 1,000,000 parts = R_{mag}
(i.e. 100 ppm = 100 / 1,000,000 = R_{mag} = 0.00010)

Eq. 2: Magnification Error in mm:
Distance (mm) from center x R_{mag} = error (mm)
(i.e. 150 mm x 0.00010 = 0.015 mm)

Eq. 3: Convert (mm) to (µm):
mm x 1000 = µm
(i.e. 0.015 mm x 1000 = 15 µm)

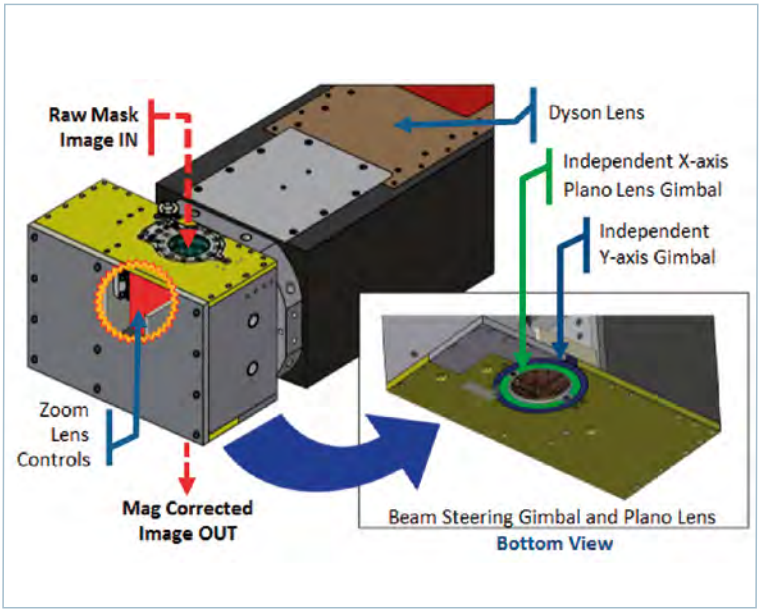

Figure 4 *Zoom lens and beam-steering hardware locations on Dyson lens*

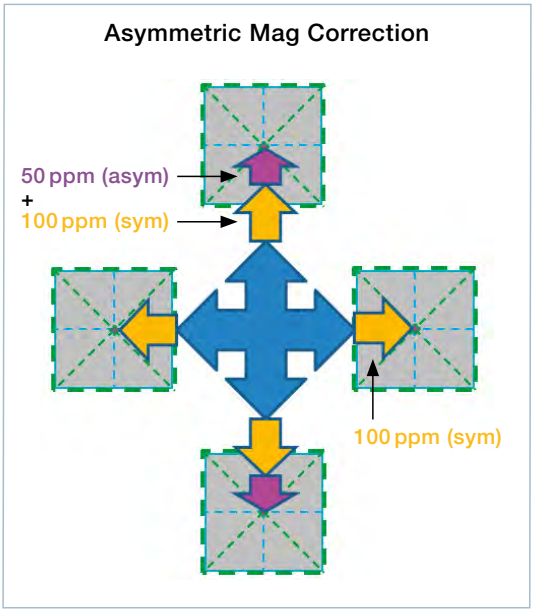

Figure 5 *Illustration of asymmetric mag correction (100 ppm in X, 150 ppm in Y)*

TECHNOLOGY

The active, wafer-to-wafer, magnification adjustment is achieved with the combination of an optical zoom lens and a novel dual-gimbal beam-steering system integrated into the DSC300 Gen3 Scanner's Wynne-Dyson projection lens. The related hardware and its locations are shown in Figure 4.

The system calculates magnification correction factors for image size and shifted die locations. The optical zoom lens adjusts the raw mask image size accordingly (smaller, larger, no action), then the independent (X & Y) gimbal mechanisms and closed-loop controls actively steer the image to the new calculated die positions.

The system can adjust for magnification up to ±200 ppm symmetric correction and ±50 ppm asymmetric adjustment.

Although, the example shown in Figure 3 only includes estimates for "symmetric" magnification (same in X and Y), the DSC300's additional capability for "asymmetric" mag correction is especially valuable because die positional errors on fan-out wafers may very well be larger in one axis. This is mainly caused by the behavior of the mold compound, such as its interaction with the temporary carrier wafer, the molding uniformity, molding temperature, EMC flow during compression, and others.

For the example of 100 ppm mag in X, and 150 ppm mag in Y (Figure 5), a residual mag of 50 ppm would remain in Y if only symmetric mag correction were applied. The benefit of symmetric and asymmetric mag correction is the full compensation for this uneven magnitude of overlay diminishing errors (100 ppm symmetric + 50 ppm asymmetric).

THEORY OF OPERATION

The ***Optical Magnification Zoom Optics*** are used to adjust the projected mask image size to match the actual die locations on the wafer. The amount of magnification difference between the mask and the wafer is determined during the global alignment step. Symmetric mag correction only needs a minimum of two alignment targets. Asymmetric mag correction requires four targets to calculate independent X and Y magnifications.

- If dies are ***closer together*** on the wafer than on the mask, then the optics components are automatically adjusted to **shrink the mask image** (Figure 6)
- If dies are ***further apart*** on the wafer than on the mask, then the optics components adjust to **grow the mask image** (Figure 6)

The system automatically sends the magnification correction factor data to both the zoom optics and beam-steering controls. The image magnification is adjusted once for each wafer, and then remains constant over the entire wafer – only the beam-steering mechanisms move during the scan exposure.

The ***Active Beam-Steering System*** cannot be separated from the ***Optical Magnification Zoom Optics***, as they must work in unison to achieve the desired results for full-field projection imaging.

Two independent precision gimbal mechanisms and closed-loop controls are used to steer the mag-corrected exposure beam in the x and y axes to compensate for the expanded or contracted die positions on the wafer.

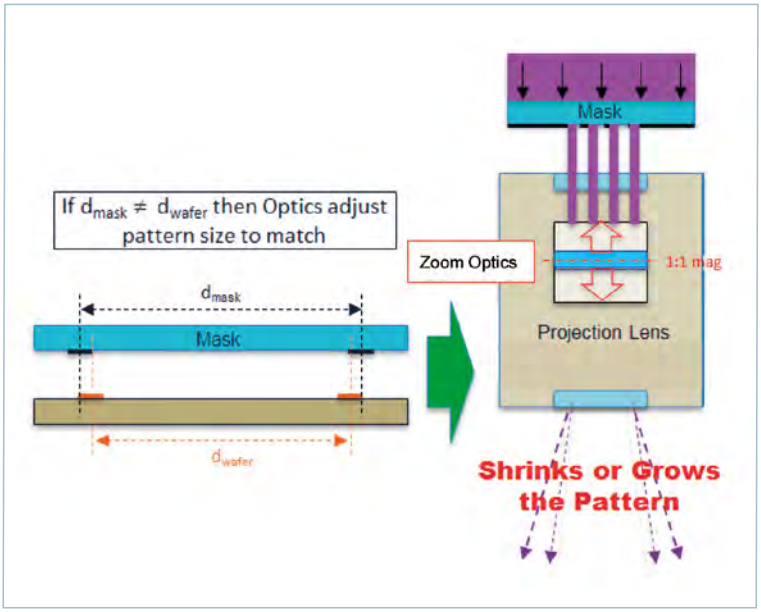

Figure 6 *Conceptual diagram of zoom optics shrinking or growing the mask pattern*

Since magnification (expansion/contraction) radiates from the center of the wafer, it is important to remember that the center die on the wafer experiences zero (0) mag error (Figure 3). Correspondingly, for beam steering:

- **Center row on wafer experiences no Y-axis magnification error**
- **Center column on wafer experiences no X-axis magnification error**

X-Axis Beam-Steering (X scans)

Figure 7 illustrates how the system continuously adjusts the x-axis gimbal plano lens angle during the exposure scan to deflect the mag-corrected image to the actual die positions (die shift compensation).

Note that the depicted angles are highly exaggerated for clarity. The angles are actually too minute to cause any image distortion or keystone effects.

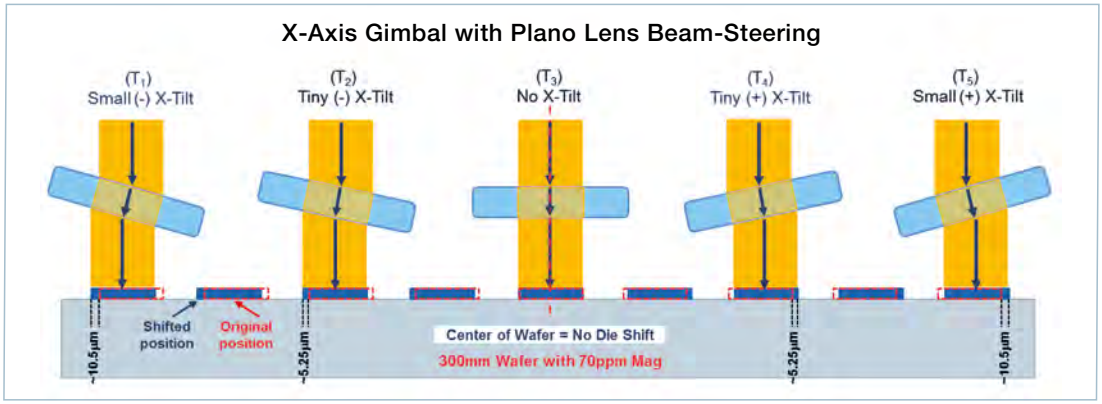

Figure 7 *Conceptual diagram of independent X-axis Plano Lens Gimbal mechanism with angles adjusted to compensate for actual die positions (blue) vs. expected locations (red dashes) at five (5) different points in time during the scanning exposure (row scan)*

In this example, at time (T_1) the translation stage has moved the left-side of the wafer under the projection optics. The plano lens angle is pre-adjusted to deflect the image toward the outside edge of the wafer by the maximum die shift amount (corresponding to 70 ppm of magnification at a distance of approximately 150 mm from wafer center).

As the stage moves the wafer closer to its center (i.e. time T_2), the lens angle is decreased proportionately. At time (T_3), the wafer center is under the lens and no deflection angle is needed or applied. As the stage moves the wafer toward its right edge, the plano lens angle is deflected proportionately in the opposite direction.

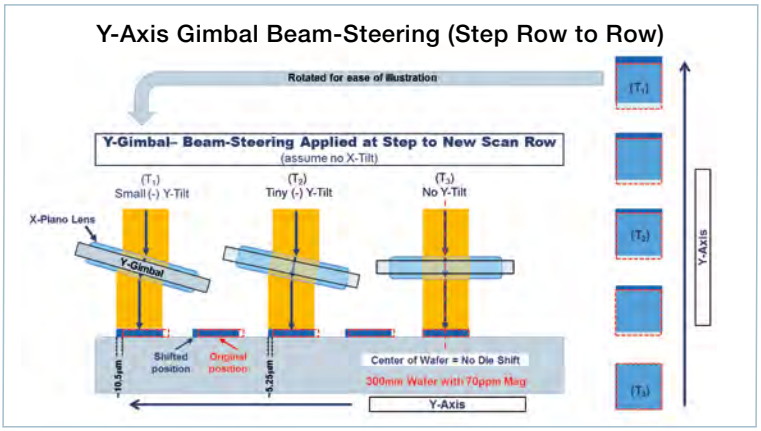

Y-Axis Beam-Steering (Y steps)

The y-axis beam-steering for die shift compensation (toward the top and bottom of the wafer) works conceptually the same as the x-axis beam steering; except the y-axis gimbal angle adjustments only happen when stepping from one row to the next. The y-gimbal angle stays fixed during the exposure scan across the row.

Figure 8 illustrates the y-axis gimbal angle adjustment for two locations: wafer center (zero deflection) and for top wafer edge (deflected proportionately for 150 mm from center.). The angle is adjusted for each row-step away from wafer center. For clarity, the x-gimbal plano lens is depicted in the zero-deflection position (not visible in side views). Note that the wafer image is rotated 90° in relation to that shown in Figure 7.

Figure 8 *Conceptual diagram of independent Y-axis Gimbal mechanism with angles adjusted to compensate for actual die positions (blue) vs. expected locations (red dashes).*

DESIGN OF EXPERIMENT

Goal:

The goal of the experiment is to prove that the projected image on the DSC300 Scanner platform can be accurately shifted by a designated off-set value and direction, as would be necessary during full-field scanning magnification correction.

Tests:

1. Zero Mag Control Test
2. Beam Shift Test: +40 ppm Mag
3. Beam Shift Test: -40 ppm Mag

Equipment:

- SUSS DSC300 Gen2 Projection Scanner System
- Above equipped with the SUSS prototype mag correction and beam steering module

Methods:

All wafers:
- 300 mm dia. silicon wafers were coated with thin resist (1 µm)
- Coated wafers were exposed with Layer-1 (L1) Vernier Test Mask pattern (± 7 µm in 1 µm increments) with zero (0) mag
- L1 exposed wafers were developed and returned to the DSC300 scanner for exposure with Layer-2 Vernier Test Mask pattern (± 7 µm in 1 µm increments)

Test #1 wafers:
exposed with 0 ppm mag offset
Test #2 wafers:
exposed with +40 ppm mag offset
Test #3 wafers:
exposed with -40 ppm mag offset

All wafers:
- Developed and sent for metrology
- Imaged with an optical microscope at five locations on each wafer (center, top, left, right, and bottom)

- ***Note: Test locations for top, left, right and bottom are 140 mm from center of wafer***

EXPERIMENTAL RESULTS

Results of 0 ppm Beam Shift Test

The printed Layer-1 and Layer-2 vernier sets indicated 0 µm shift, which are successful results for 0 ppm mag. Vernier images are omitted for space saving reasons.

Results of +40 ppm Beam Shift Test

Evaluation Methods

The relative positions of the Layer-1 and Layer-2 vernier patterns were evaluated at four different locations on the test wafer (top, left side, right side and bottom).
The magnitude of the image shift was determined by finding the set of vernier marks (Layer-1 and Layer-2) that were most “in line” with each other (best overlapping). If there were two sets of “best overlapping” vernier marks, the magnitude was interpreted as being between the two values for the sets of marks (N_1-N_2).

The direction of the image shift was determined by comparing the relative positions of the Layer-2 vernier marks to the Layer-1 vernier marks (i.e. the Layer-2 marks were shifted “in” toward the center of the wafer = negative (-) direction).

.

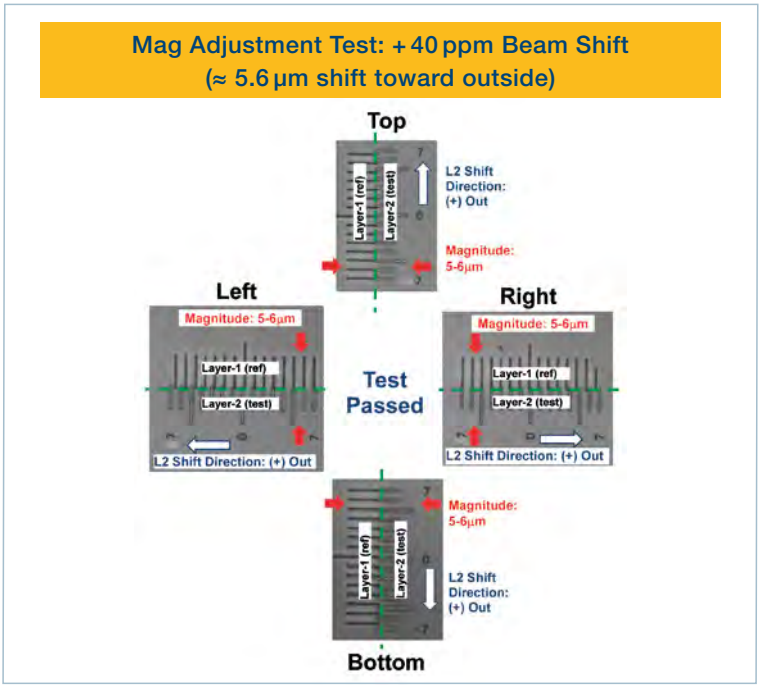

Figure 9 *Optical images of overlapping vernier patterns (Layer-1 and Layer-2) at four locations on test wafer (top, left, right, bottom)*

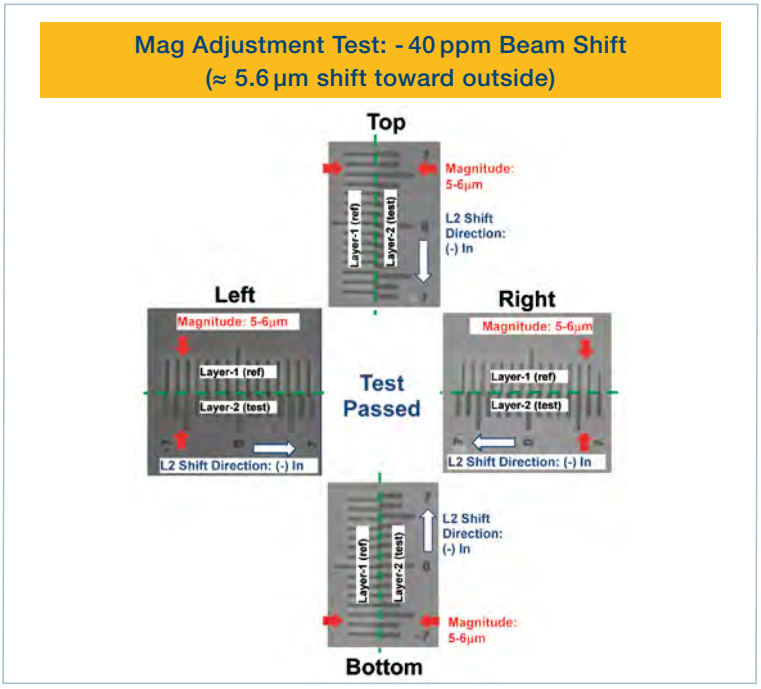

Figure 10 *Optical images of overlapping vernier patterns (Layer-1 and Layer-2) at four locations on test wafer (top, left, right, bottom)*

Expected Results

Magnitude of Shift: ≈5.6 µm
Each of the four test points on the wafer were 140 mm from the center, so with (+40 ppm) magnification the shift should be ≈5.6 µm.

Direction of Shift: For positive (+) magnification the image shift should be "out" toward wafer's perimeter.

Target Magnification: +40 ppm in X & Y

Actual Results (Figure 9)

Magnitude of Shift: **5-6 µm**
(the vernier set for 5 µm and the vernier set for 6 µm were both in good alignment)

Direction of Shift: **"Out" toward edge (+ pos)**

Magnification Measured by DSC300:

- ***X-axis: +40.0 ppm***
- ***Y-axis: +41.5 ppm***
- ***Target achieved within 1.5 ppm (0.21 µm)***

Results of -40 ppm Beam Shift Test

Evaluation Methods

The same evaluation methods used for the +40 ppm Beam Shift Test were used.

Expected Results

Magnitude of Shift: ≈5.6 µm
Each of the four test points on the wafer were 140 mm from the center, so with (-40 ppm) magnification the shift should ≈5.6 µm.

Direction of Shift: For negative (-) magnification the image shift should be "in" toward the wafer's center.

Target Magnification: -40 ppm in X & Y

Actual Results (Figure 10)

Magnitude of Shift: **5–6 µm**
(the vernier set for 5 µm and the vernier set for 6 µm were both in good alignment)

Direction of Shift: **In toward center (- neg)**

Magnification Measured by DSC300:

- ***X-axis: - 43.2 ppm***
- ***Y-axis: - 42.0 ppm***
- ***Target achieved within 3.2 ppm (0.45 µm)***

ANALYTICAL RESULTS

Multiple analytical tests were performed and data analyzed to determine if the use of *Magnification Correction* and *Beam-Steering* had any impact on:

- Overlay accuracy
- CD stability
- Resolution loss

Overlay Accuracy Check

Metrology

The same 25 points on each of the three test wafers (0 Mag, + 40 Mag and - 40 Mag) were manually measured with an optical microscope. The overlay data was plotted separately for the x-axis and for the y-axis. Each chart shows the results for all three test wafers, side by side for easy comparison (Charts 1 and 2).

Evaluation Method

The plotted overlay results for the two test wafers with mag correction processing (+ 40 ppm Mag and - 40 ppm Mag) were compared against the results from the control wafer (No Mag – 0 ppm).

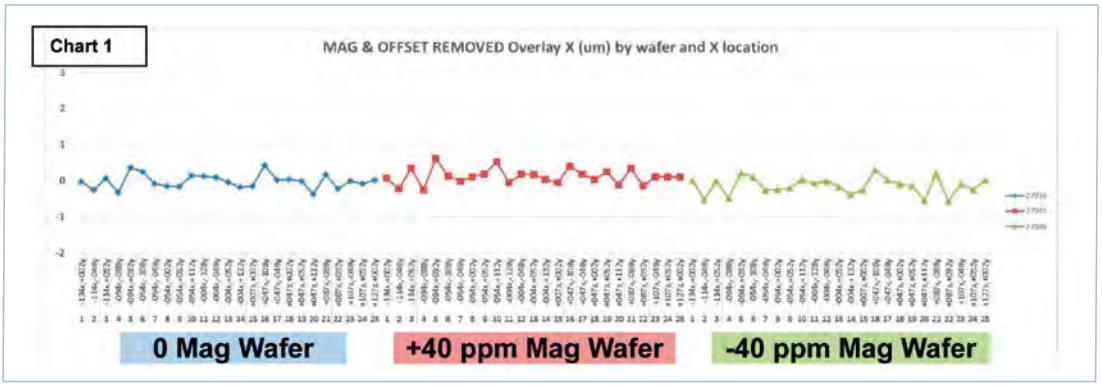

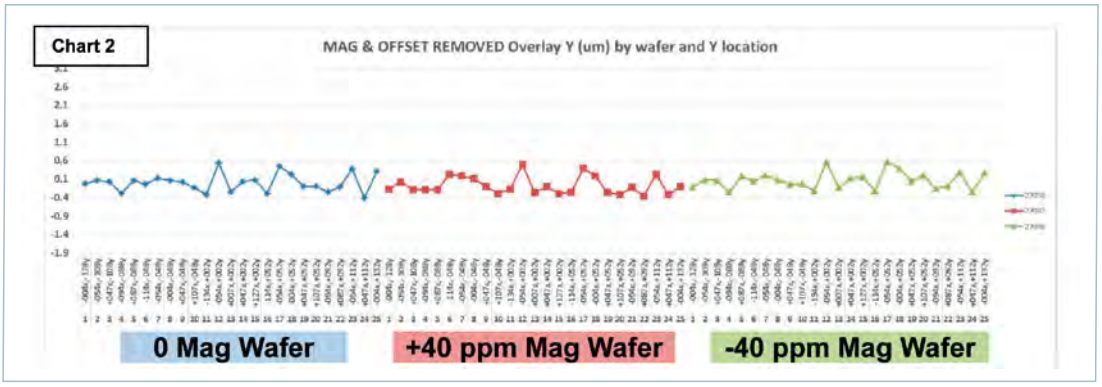

Chart 1 *(Top) Plot of X-overlay data for all three test wafers, side by side*
Chart 2 *(Bottom) Plot of Y-overlay data for all three test wafers, side by side*

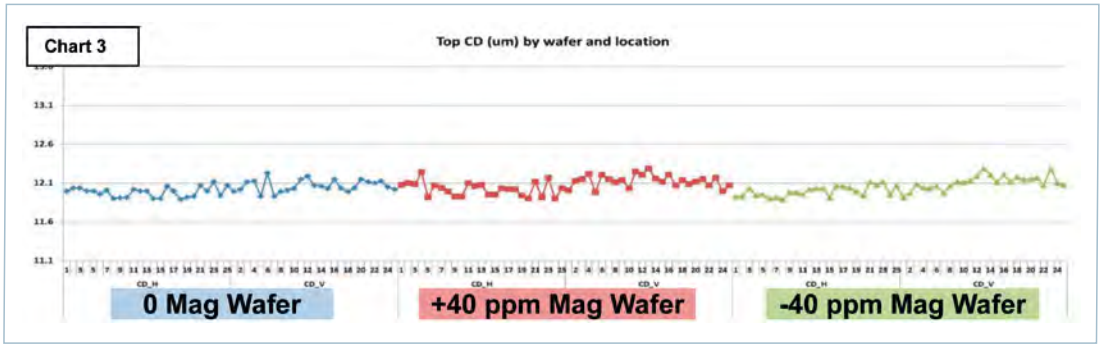

Chart 3 *Plot of CD (µm) data for all three test wafers, side by side*

Conclusions of Test

- Mag correction and beam-steering did not adversely impact the overlay on the two test wafers
- All three wafers showed the same stable overlay performance

CD Stability Check

Metrology

For all three test wafers (0 Mag, +40 Mag and -40 Mag) the CD (both X & Y) were manually measured with an optical microscope at the same 25 locations. The CD data (50 measurements) was plotted for all three test wafers, side by side for easy comparison (Chart 3).

Evaluation Method

The plotted overlay results for the two test wafers with mag correction processing (+40 ppm Mag and -40 ppm Mag) were compared against the results from the control wafer (No Mag – 0 ppm).

Conclusions of Test

- Mag correction and beam-steering did not adversely impact the CD Stability on the two test wafers
- All three wafers showed the same overall magnitude of stability

Resolution Loss Check

Metrology

For all three test wafers (0 Mag, +40 Mag and -40 Mag) the imaged 2 µm L/S Test Patterns were imaged with an optical microscope (OM), at the same locations (Figure 11).

Evaluation Method

The OM images for the two test wafers with mag correction processing were visually compared against the image from the control wafer (No Mag – 0 ppm).

Conclusions of Test

- Mag correction and beam-steering did not create any discernable resolution loss
- All three wafers showed that 2 µm resolution was clearly achieved

CONCLUSION

Overlay accuracy is more critical than ever with the proliferation of fan-out wafer level packaging technology. Systematic magnification errors – whether induced by the fan-out process or thermal conditions during exposure – are a significant portion of the overlay budget. Die positional magnification for fan-out wafers is reported to span

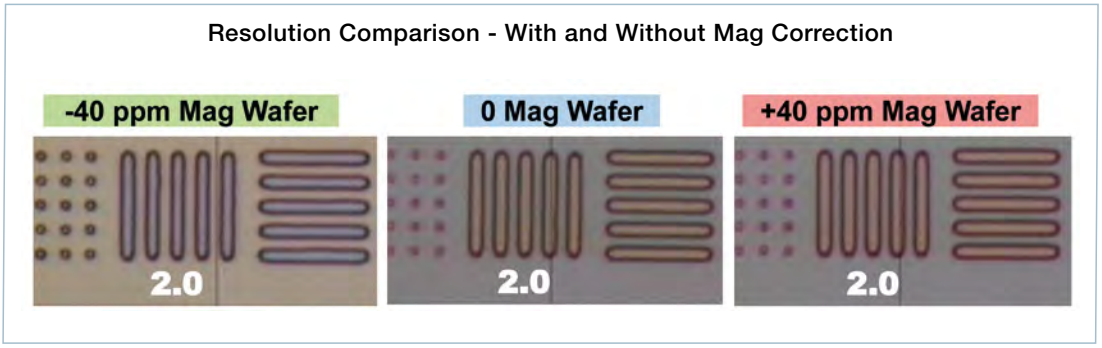

Figure 11 *Optical microscope images of 2 µm L/S resolution pattern on the three test wafers*

from 10's of ppm to 100's of ppm [2]. Mitigating all or most of the systematic magnification errors (symmetric or asymmetric) for fan-out wafers with magnification correction technology on the DSC300 Gen3 full-field exposure system is an efficient strategy for improving overlay [1], while maintaining a high throughput and a low cost of ownership.

SUSS MicroTec has demonstrated the proof-of-concept for its *Optical Magnification Correction and Beam-Steering* technology. This novel technology will be applied to its DSC300 Gen3 full-field projection scanning lithography platform. It was shown that target magnification adjustments were achieved with sub-micron accuracy, without degradation of overlay, CD stability or fine resolution.

The DSC300 Gen3 Full-Field Projection Scanner with ± 200 ppm symmetric and ± 50 ppm asymmetric magnification correction is scheduled for release in Q2/2018, at a lower-than-stepper capital cost and a much faster-than-stepper throughput for an outstanding low cost-of-ownership.

Acknowledgements

The authors would like to acknowledge the SUSS MicroTec Photonic Systems engineering team for their innovation and for supplying the test data for this article. And, special thanks to Uwe Vogler (SUSS MicroOptics, S.A.) for performing the experimental tests and compiling the data.

References

[1] *B.W. Smith and K. Suzuki, "Alignment and Overlay," in Microlithography: Science and Technology, 2nd ed. Boca Rotan, CRC Press, 2007, Vol. 126, sec. 1.8, pp. 46-48*

[2] *S. Yeon et. al., "Compensation Method for Die Shift Caused by Flow Drag Force in Wafer-Level Molding Process," Micromachines 2016, 7, 95; doi:10.3390/mi7060095, pg. 7*

[3] *R.L. Hsieh et. al., "Lithography Challenges and Considerations for Emerging Fan-Out Wafer Level Packaging Applications," in Proceedings of the International Wafer Level Packaging Conference*
Conference (IWLPC), San Jose, CA, USA, 11-13 November 2009; pg. 5

Matthew Gingerella is the International Product Specialist for SUSS MicroTec Photonics Systems (SMTPS), with over 10 years combined Tamarack / SUSS product and application experience.
He earned a Bachelor of Arts degree in chemistry at California State University Fullerton, to compliment his 2-year degree in electronics / computer technology.

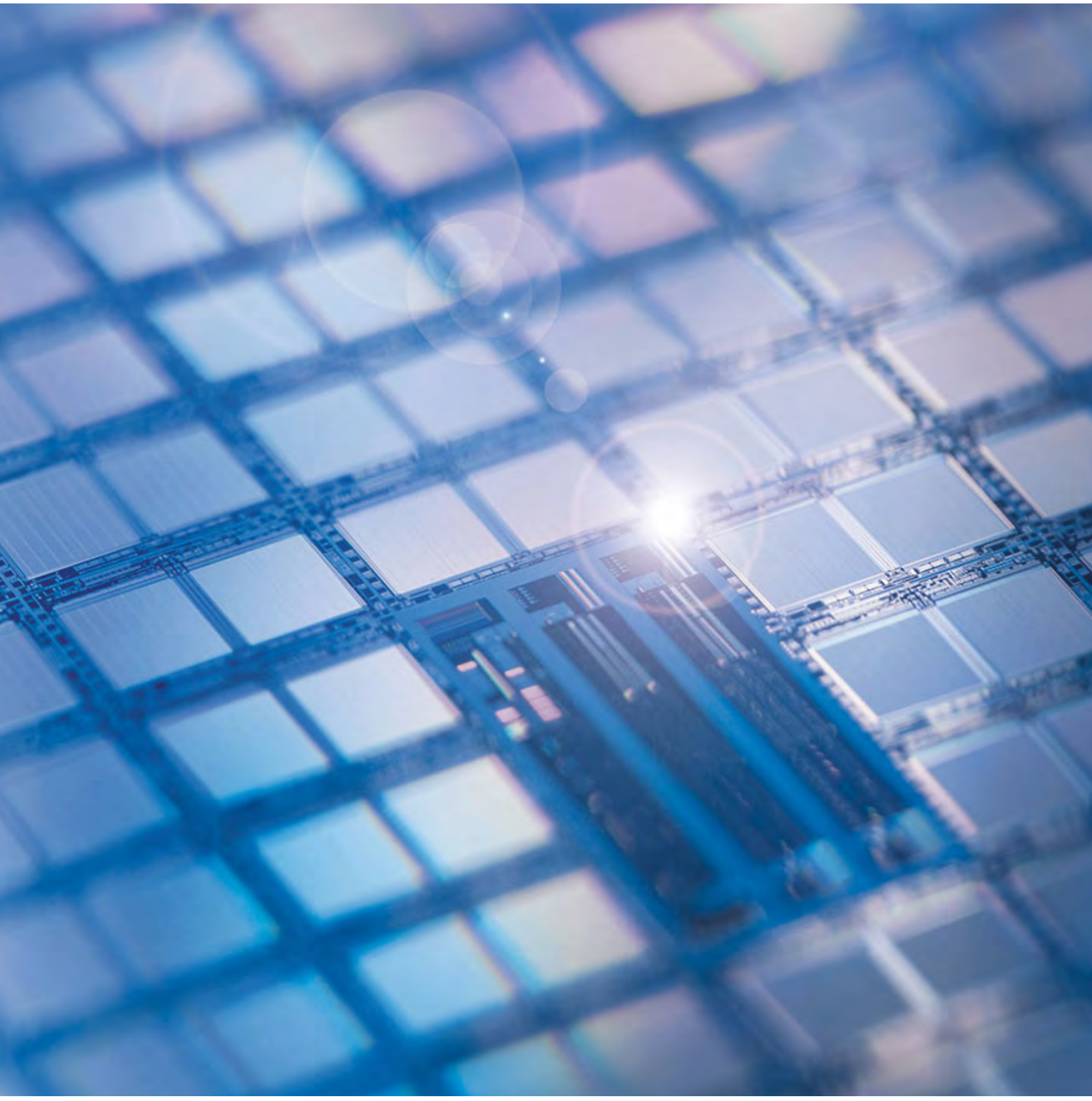

LASER PRE-BONDING AS A NOVEL METHOD FOR IMPROVED POST-BOND ALIGNMENT ACCURACY IN SILICON-TO-SILICON METAL BONDING

Hiroyuki Ishida Manager, Business Development Wafer Bonding, SUSS MicroTec KK
Dr. Tim Griesbach Senior Application Scientist Bonder, SUSS MicroTec Lithography GmbH
Stefan Lutter General Manager Bonder, Coater / Developer, SUSS MicroTec Lithography GmbH

In order to realize further miniaturization and allow more freedom to MEMS chip design, improvement of post-bond alignment accuracy is beneficial. In current MEMS packaging processes, post-bond alignment accuracy is typically around 5 -10 µm (or even worse) and is influenced by several factors such as not only the bonding process itself but also the handling and transfer of the aligned wafer pair, thermal effects that occur during loading the wafers onto a pre-heated bonding chuck or ramping the temperature during the bonding process. In addition, wafer shift can also occur during the removal of spacer flags that are used to keep wafers in separation during the pump down steps or squish of the bond lines when the bond force is applied at elevated temperature.
To keep wafer-to-wafer alignment throughout bonding process, laser pre-bonding has already been employed in production of silicon-to-glass triple-stack anodic bonding. On the other hand, metal bonding, such as Au-Au and AlGe, is getting more attractive due to its useful features like thin bond line for good hermetic sealing and enabling electrical connection. In order to achieve excellent post-bond alignment accuracy in metal bonding, we have developed a novel and innovative method, or silicon-to-silicon laser pre-bonding, which overcomes these aforementioned issues by locking the alignment between the wafers prior to transferring them into the bond chamber. Some studies have been done so far using laser-assisted bonding, however, they were not for improving alignment accuracy but for creating actual bonding of bond lines [1, 2]. This novel method provides a significant improvement in post-bond alignment accuracy and can be applied to a variety of bond line materials that are used in recent MEMS applications.

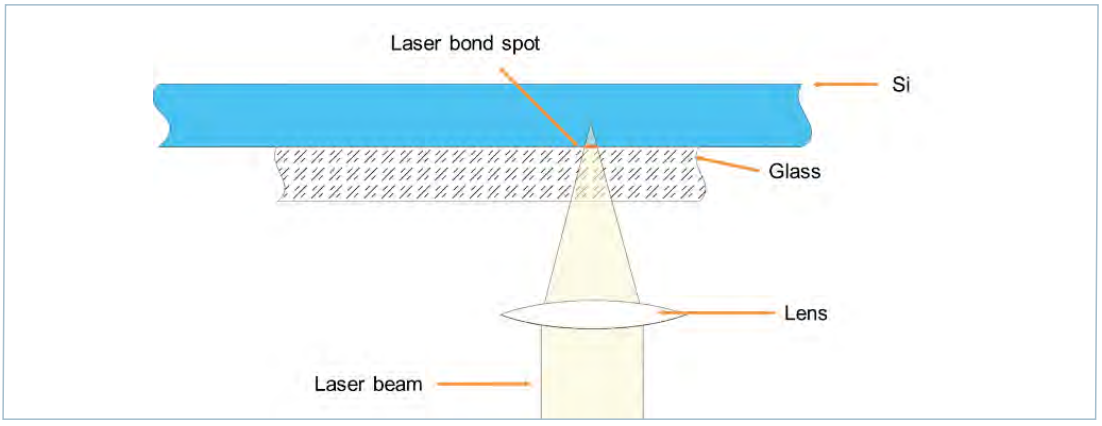

Figure 1 *Schematic of silicon-to-glass laser pre-bonding set-up*

SILICON-TO-GLASS LASER PRE-BONDING

SUSS MicroTec initially developed laser pre-bonding technology on BA 6 / 8 bond aligner systems more than 10 years ago for silicon-to-glass bonding. Figure 1 shows a schematic of silicon-to-glass laser pre-bonding set-up. The technology has been used in production of a triple-stack

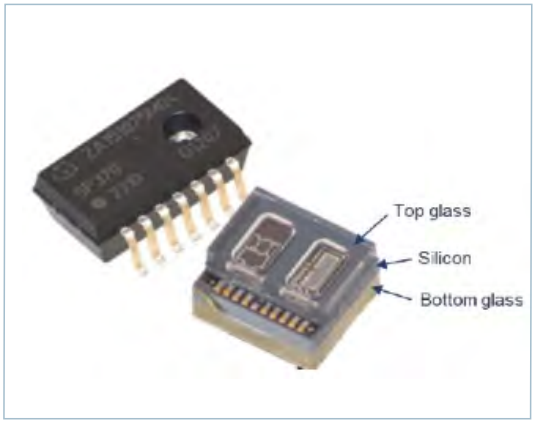

Figure 2 *MEMS pressure sensor product employing laser pre-bonded triple stack anodic bonding*
(Source: http://www.systemplus.fr/reverse-costing-reports/infineon-sp37-tire-pressure-monitoring-sensor/)

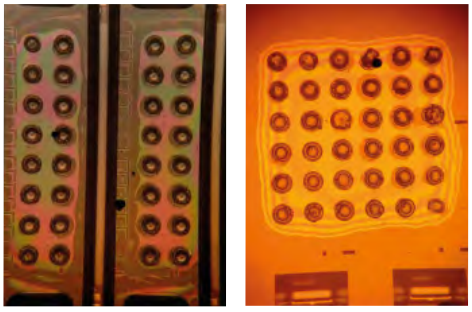

Top Bond
Pre-bond & Anodic Bond

Bottom Bond
Pre-bond & Anodic Bond

Figure 3 *Silicon-to-glass laser pre-bonding spots*

anodic bonding (glass - silicon - glass) of MEMS pressure sensors (Figure 2) on fully automatic SUSS bonders for many years.

A Nd:YAG IR laser (λ = 1064 nm) has been employed, whose wavelength is absorbed in silicon and allows "spot welding" of glass to silicon wafer without any intermediate layer. The size of a typical bond spot is about 500 µm and the bond force is around 50 grams or 0.49 N. Usually, laser pre-bonding is performed as spot array (e.g. 2 x 8, 6 x 6 as shown in Figure 3) to obtain sufficient bond strength to fix two wafers.

In triple-stack bonding, both glass wafers undergo sequential laser pre-bonding to the silicon wafer prior to "2-in-1" anodic bonding for making the final triple-stack sandwich structure.

Post-bond alignment accuracy (factor of 3x - 4x) and throughput ("2-in-1" process) were significantly improved compared to sequential anodic bonding with traditional wafer transfer of non-pre-bonded wafers after alignment.

TRANSFER OF PROVEN METHOD TO SILICON-TO-SILICON LASER PRE-BOND

In order to apply this laser pre-bond technology to silicon-to-silicon metal bonding, a different laser wavelength, with very high transmission through silicon has been selected, so that no energy is absorbed in bulk silicon.
Since the laser light is not absorbed by silicon and almost no heat is generated at the bonding interface, therefore a good light absorption layer such as Ti, TiW, TiN, Ta, TaN is inserted under the bonding interface. On top of this absorption layer, also acting as an adhesion / barrier layer, the bonding layer like Cu, Au, Al or AlGe is formed.
When laser energy is absorbed in the absorption layer material, it melts the metal layer(s) and forms a pre-bond spot.

PRELIMINARY EXPERIMENT OF SILICON-TO-SILICON LASER PRE-BOND

Silicon-to-silicon laser pre-bonding was performed for Au-Au bonding test wafers using an IR laser. Metal layer structure was Ti 125 nm / Au 1.5 µm on both wafers, where Ti is used as the light absorbing layer to generate heat. The laser pulse has the power of 70 W with the typical spot diameter of 240 µm and the irradiation duration was 0.5 s for each laser spot. Figure 4 shows a schematic of the setup of Si-to-Si laser pre-bonding. In the actual case on the SUSS XBS200 (Figure 5), wafer-to-wafer alignment was performed on the XBA bond aligner module by ISA (inter-substrate alignment) method and then laser was irradiated to the target position on the wafer center area with maintaining the alignment.

As shown in Figure 6, laser shots can create melting zones which depend on absorption properties of the absorbing layer and laser energy. Repeat test with Ti / Au bond line for 10 samples and 2 x 2 laser pre-bonded dot matrix shows tensile force of 22 N +/- 1.7 N, that is about 40 times of the weight of a standard 200 mm Si wafer. This means that this laser pre-bonding can securely hold a 200 mm Si wafer and maintain alignment as well. Figure 7 shows the SAM images (a) after laser pre-bonding and (b) after final Au-Au bonding at 400° C. The imprint of 2 x 2 laser pre-bonding spots could be re-diffused and was completely disappeared after the bonding step.

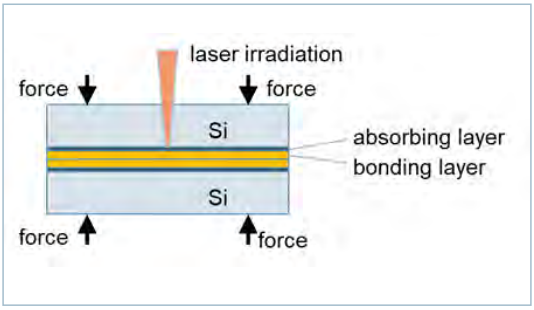

Figure 4 *Schematic of silicon-to-silicon laser pre-bonding set-up*

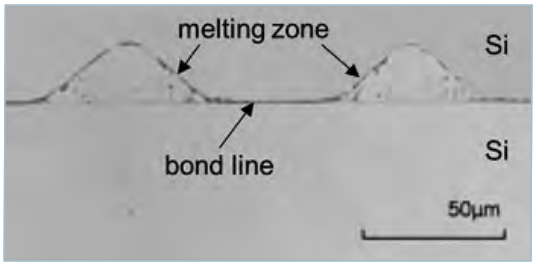

Figure 6 *Cross-sectional SEM image of the laser pre-bonded area. Si melting zone can clearly be seen*

Figure 5 *SUSS XBS200 automated wafer bonder*

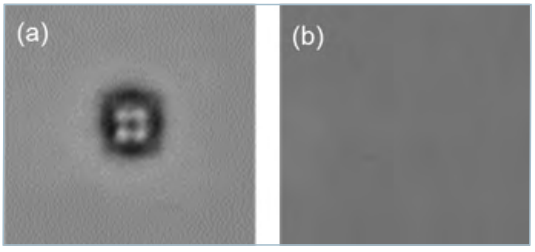

Figure 7 *SAM images (a) after laser pre-bonding (2 x 2 laser spots) and (b) after final Au-Au bonding at 400° C*

CONCLUSION

Laser pre-bonding has been successfully used in production as a post-bond alignment improvement method for silicon-to-glass bonding so far and now is going to be applied extendedly to silicon-to-silicon metal bonding processes.
Si-to-Si laser pre-bonding was successfully performed by using an IR laser. The bonding strength of a 2 x 2 spot array was around 22 N which is sufficient to maintain the wafer pair in contact without any alignment shift. In Au-Au bonding, laser pre-bonded spots have disappeared after the final bonding step at 400° C. This laser pre-bonding can achieve excellent post-bond alignment accuracy which leads to die cost reduction and improvement of the flexibility of chip design.

References

[1] *N. Lorenz, M. D. Smith, D. P. Hand, "Low temperature wafer-level packaging of MEMS using selective laser bonding," Proceedings of 29th International Congress of Applications of Lasers and Electro-Optics, ICALEO 2010, Anaheim, CA, USA, Sep. 26-30, 2010, pp. 871-876, (2010)*

[2] *Y. Tao, A. P. Malshe, W. D. Brown, "Selective bonding and encapsulation for wafer-level vacuum packaging of MEMS and related micro systems," Microelectronics Reliability, 44 (2), pp. 251-258, (2004)*

Hiroyuki Ishida joined SUSS MicroTec KK in 2006 as a senior application engineer and then worked as a business development manager in Japan mainly focused on wafer bonding applications.
He is now the manager of business development wafer bonding, being responsible in applications and sales support related to permanent bonding and temporary bonding / debonding products. He is also taking care of the collaboration with Japanese material suppliers for temporary bonding applications.
He received his B.E. and M.E. in Electronic Engineering from Tohoku University.

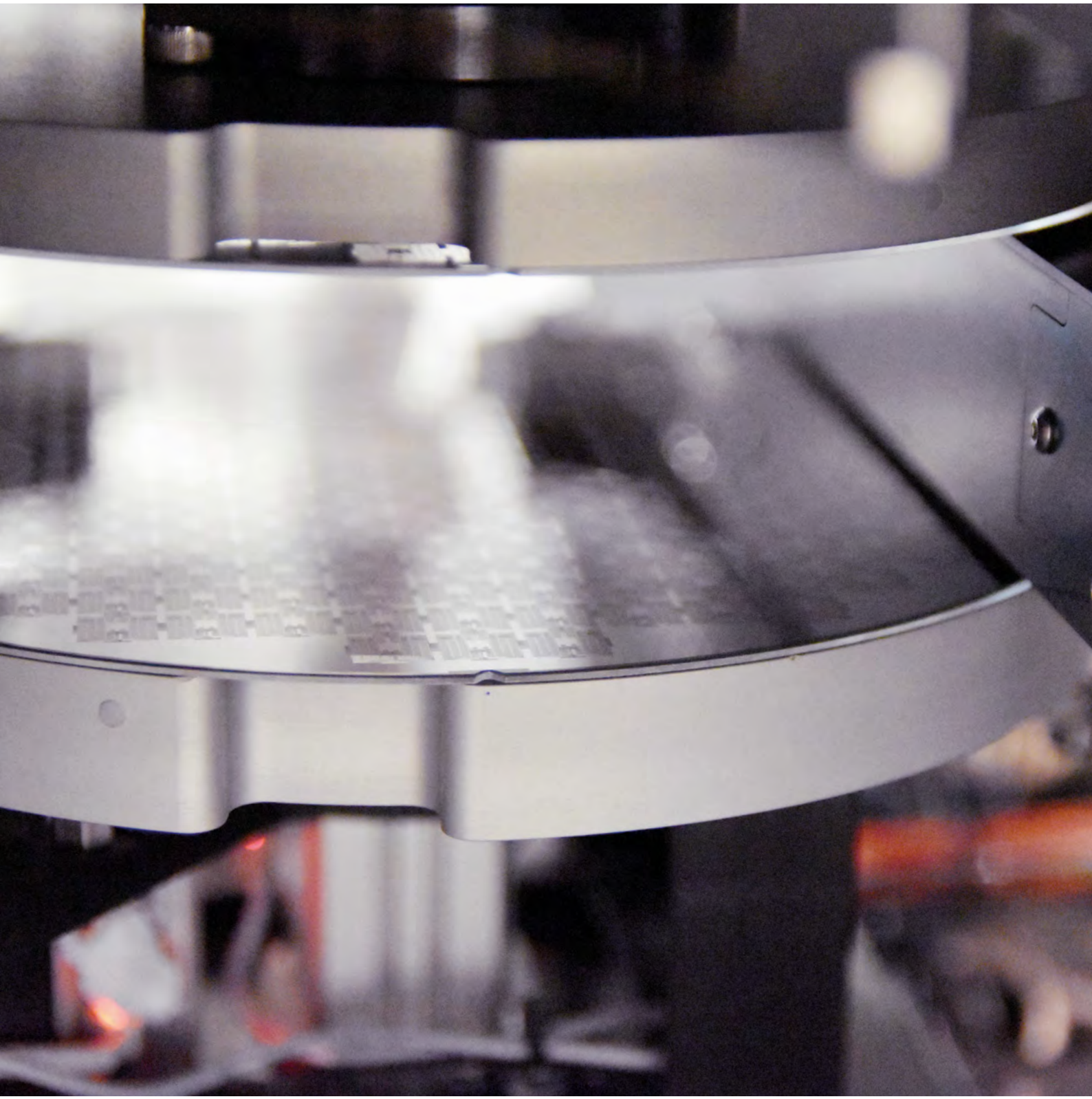

HIGH INTENSITY UV-LED MASK ALIGNER FOR APPLICATIONS IN INDUSTRIAL RESEARCH

Katrin Schindler SUSS MicroTec Lithography GmbH, Schleissheimerstr. 90, 85748 Garching, Germany
U. Leischner, P. Kaiser, T. Striebel, U. Schömbs SUSS MicroTec Lithography GmbH, Schleissheimerstr. 90, 85748 Garching, Germany
C. Lopper Fraunhofer IZM, Gustav-Meyer-Allee 25, 13355 Berlin, Germany

Recent rapid technological progress in the field of UV-light emitting diodes promises great opportunities. Ecological UV-LED light sources can replace traditional mercury lamps with tremendous less power consumption, no hazardous waste and no need for special safety measures [1]. Moreover, new processes and applications become possible thanks to the unprecedented flexibility in illumination control.
Already today UV-LEDs offer a cost-effective, green and flexible replacement for Hg-lamps in main-stream water purification, counterfeit detection and curing applications. First benchtop lithography investigations with UV-LEDs date back to 2005 [2]. Since then many research teams working on a multitude of materials have demonstrated good print performance of UV-LEDs in all types of lithographic processes [3-7]. However, they also showed that the limits of home-made benchtop setups needed to be overcome to qualify UV-LED illumination for commercial lithographic manufacturing.

In this paper we show first results on a semi-automatic mask aligner with UV-LED illumination, SUSS MA/BA8 Gen4 *Pro* equipped with a UV-LED lamp house and MO Exposure Optics [8]. The tool offers a customer-controllable spectrum with three wavelengths corresponding to the mercury i, g and h-line. The field-proven MO Exposure Optics guarantees a reliable smooth angular spectrum that can be fully customized. Full 8 inch wafers were exposed with the same high intensity and light uniformity as with standard 1 kW mercury lamps. Broadband and single line exposures were performed on several standard processes. The resolution and appearance of the produced features compared well to traditional exposures with a mercury lamp.

In addition we present an analysis of the eco-fingerprint of our UV-LED-lithography system. For a semi-automatic system used under typical research institute conditions the LED light source can survive a machine life-time. LEDs don´t require warm up times and thus are switched on during exposure only. Moreover, low power consumption of the LEDs during operation and no need for nitrogen flow cooling also contribute to very low running cost and a green footprint.

In summary, the lithography industry will greatly benefit from UV-LED illumination paving the way for future process innovations in a mercury-free and safe environment.

INTRODUCTION

Ecological and safety concerns call for a reliable and energy effective replacement of mercury lamps in lithographic applications. Many researchers have already shown good print performance of UV-LEDs in laboratory test setups [2-7, 9-10]. To qualify UV-LED illumination for commercial lithographic manufacturing reliable machine integration, high intensities, good light uniformity [7,9], reproducible dose and illumination conditions [10] and control of the angular spectrum [5] are necessary.

Here, we compare the lithographic performance of a standard 1 kW mercury lamp with a multi-wavelength UV-LED source with essentially identical light intensity. In addition, we discuss the typical wavelength spectrum of the UV-LED source and its user customizable composition and present the results of lithographic exposures and imprints on full 8 inch wafers. We demonstrate that the light source choice has no significant impact on pattern resolution and appearance. Further, an investigation of its eco-finger-

print reveals that the UV-LED source reduces the mask aligner energy consumption.

FLEXIBLE WAVELENGTH SPECTRUM

Multi-wavelength UV-LED light sources imitate the emission line spectrum of mercury vapour lamps. To compare both light sources, intensity spectra of the 1 kW mercury lamp and of the UV-LED source were recorded in a wavelength range between 350 and 470 nm. Figure 3 shows a comparison of the recorded spectra. The spectrum of the MA/BA8 Gen4 *Pro* mask aligner equipped with the LED light source (solid orange line) shows light intensities of about the same magnitude (compare the area under the intensity curve around the peak wavelength) and at essentially the same wavelengths as the spectrum of the 1 kW mercury lamp (dark blue line). The recorded intensity uniformity with MO Exposure Optics [8] is better than 2.5 % for both the LED source and the mercury lamp. The LED arrays emit light around the characteristic mercury lines 365 nm (i-line), 405 nm (h-line) and 436 nm (g-line). The emission peaks are broader as compared to the mercury lamp. However, these results show that strong intensities at the sensitive regions of typical resist materials can be achieved easily with the LED light source.

In addition, the LED source offers the possibility to separately control the LED arrays. The orange solid line in Figure 3 shows a broadband UV-LED spectrum with full intensity of all three lines. A user can adapt the wavelength spectrum to a specific application (e.g. Figure 1 and 2) and store the light configuration in the machine recipe. For example, i-line exposures can be performed without filter exchange by switching on only the i-line LEDs.

In some cases the user might want to reach the best possible match to a specific best practise process. For this purpose the LED light source allows adapting the composition of the i-, h- and g-line intensities to a known mercury lamp spec-

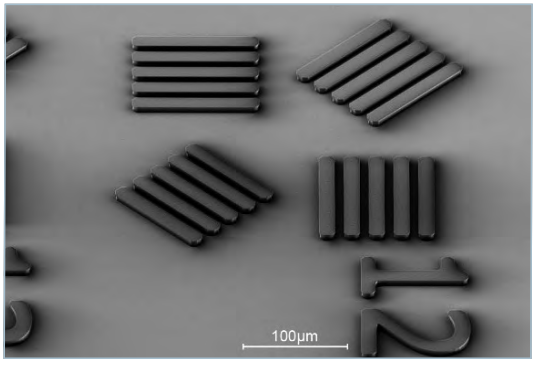

Figure 1 *UV-LED broadband exposure in 8 µm thick AZ2070nLof at 20 µm proximity gap. FIB image of 12 µm structures with Pt-coating for resist protection*

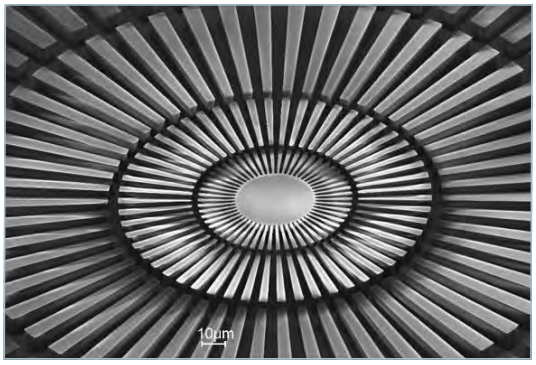

Figure 2 *SEM image depicting Siemens star pattern exposed with g-line UV-LEDs in 10 µm thick AZ9260 in hard contact mode*

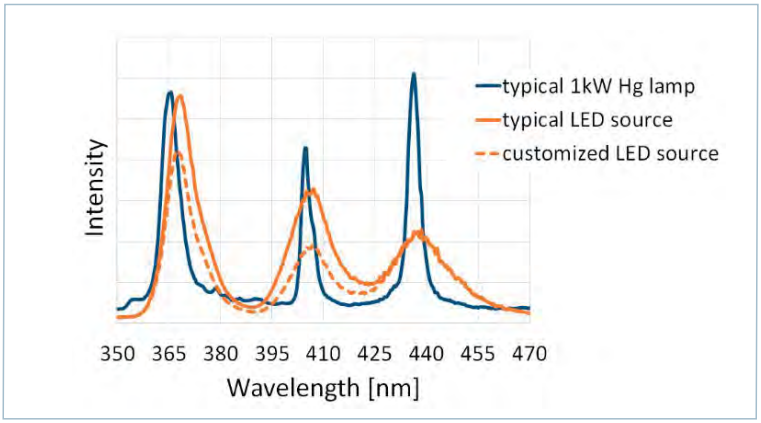

Figure 3 *Spectrum of a typical 1 kW mercury lamp (dark blue), a typical LED light source (solid orange) and example of an LED source with customized composition (dashed orange)*

trum (e.g. to a 350 W lamp or 1 kW lamp spectral composition). Here the area below the intensity-wavelength curve in Figure 3 and the spectral resist absorption characteristics of the resist [11] can be taken into account. The dashed line in Figure 3 shows the spectrum of an LED source that was adjusted to closely mimic the 1 kW lamp spectral response for AZ4110.

The flexibility in adjusting or composing the wavelength spectrum offers new opportunities. Even machine-to-machine matching of the illumination becomes possible. The MO Exposure Optics additionally guarantees a reliable smooth angular spectrum where also the exposure angle composition can be fully customized [8].

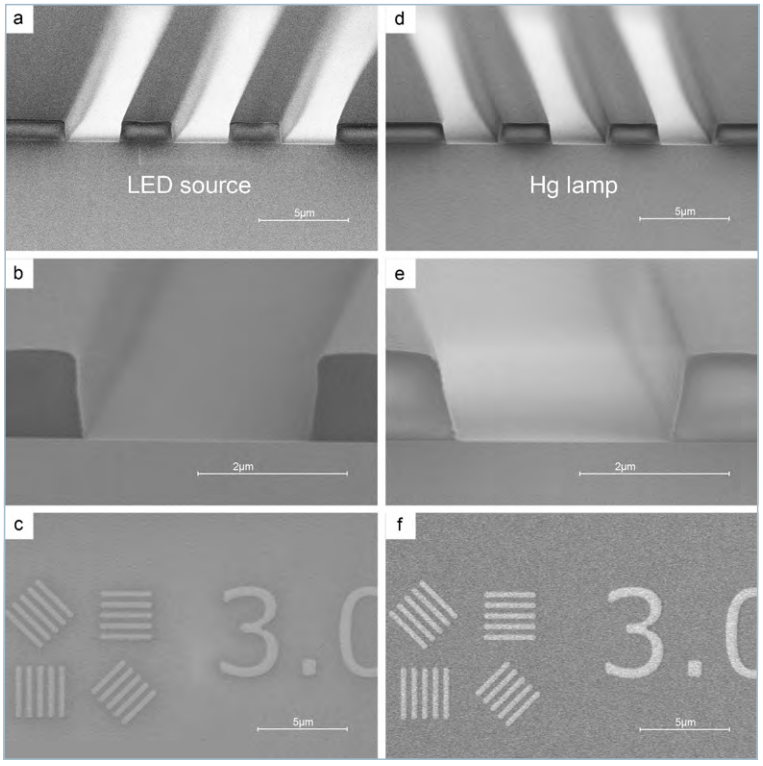

Figure 4 *Broadband exposures of 3 µm Line/Space patterns with LED source (a-c) and with mercury lamp (d-f) in 1.2 µm thick AZ4110 resist exposed at 20 µm proximity gap*

LED AND HG LAMP PRINTS MATCH

Many research groups showed that SU8 [5,7,10] and i-line resist [6] exposures can successfully be performed with UV-LEDs. Here, a test series of full 8 inch wafers with typical resists and several resist thicknesses was exposed under varying exposure conditions. For direct comparison each test was performed with the LED lamp house and with a traditional 1 kW mercury lamp under comparable conditions.

The LED spectrum was customized to closely match the 1 kW Hg lamp exposure for AZ4110 (dashed line in Figure 3). But, even in tests without customization of the LED source (maximum intensity on all i, h and g-line LEDs) no significant difference was found in feature shape and resolution.

Figure 4 shows secondary electron microscope images of Line/Space patterns produced in 1.2 µm thick AZ4110 resist with the LED source (left) and the traditional 1 kW Hg lamp (right). All three mercury lines (broadband) were used to generate the patterns. These shadow print exposures were performed with a proximity gap between mask and wafer of 20 µm. For each source we used an optimized dose as determined with test exposures. The process parameters were identical for both light sources, however no effort was taken to fully optimize the process for e.g. suppression of standing waves, best possible side wall angles or best possible resolution. Similar tests were performed with AZ4110 at other proximity gaps up to 100 µm. The smallest reproducibly resolved feature size over the whole wafer was 3 µm for exposures with 20 µm proximity gap (Figure 4) and 6 µm for 100 µm proximity gap.

Figure 5 shows SEM images of Line/Space patterns in thick resist (10 µm thick AZ9260) exposed with a large exposure gap of 100 µm, a typical process used for etch mask definition for dry etch processes or redistribution layer formation on wafers with topography. The feature shapes produced by the LED source (left) and the mercury lamp (right) are almost identical.
For additional tests with monochromatic light we used filters with the Hg lamp and selected only a single LED array, e.g. i-line, in the machine recipe of the LED tool. In all cases the feature shapes and side wall angles produced by the LED source are very similar to the mercury lamp prints. No significant impact of the light source is visible in any of the exposures neither in the feature shape nor in the resolution.
UV-LED exposures were successfully utilized in diverse other applications. Figure 6 shows an example of an array of microlenses manufactured using the SMILE (SUSS MicroTec Imprint Lithography Equipment) technology wherein the imprinting material is brought into the required 3D shape via a stamp. In this process, the illumination with UV-light triggers the cross-linking within the imprint polymer and therefore leads to its solidification. The lens array shown in Figure 6 was imprinted on 200 mm wafers using the DELO OM 6610 material. During all imprint tests, the LED source produced equivalent results compared to traditional Hg lamps. Moreover, imprint applications favor particularly high exposure doses to achieve best performances, making high power LED-sources (equivalent to 1 kW lamps) the optimal solution.

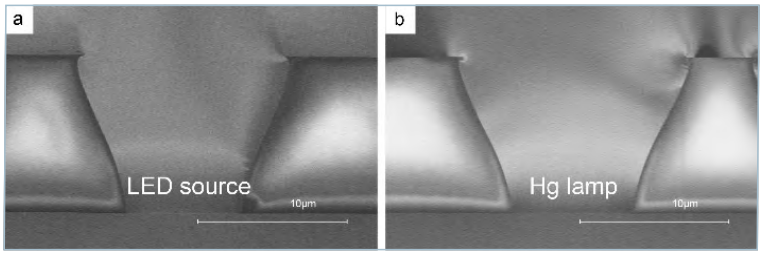

Figure 5 *Identical shape of Line/Space features in 10 µm thick AZ9260 resist exposed in 100 µm proximity gap with LED source and 1 kW Hg-lamp*

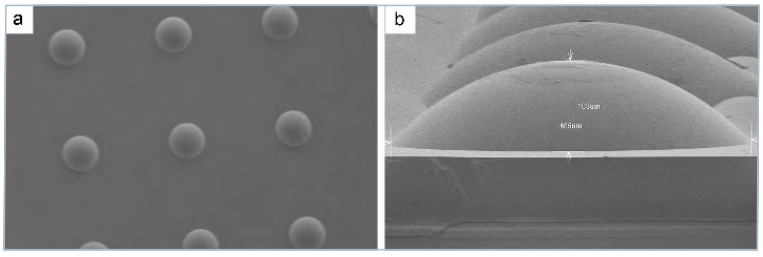

Figure 6 *Imprinted arrays of microlenses produced using SMILE technology with LED source*

ECO-FINGERPRINT

LED technology allows for the fabrication of extremely long-lasting light sources. UV-LEDs have typical life times of 5,000 to 30,000 hours. They are switched on only during the wafer exposure itself, which typically takes one to a few seconds. An LED-source module may thus last for a full manual aligner machine life of more than 10 years without the need for replacement [12].
Today's mercury lamps on the contrary have to be replaced regularly (life time 1,000 to 2,250 hrs). In a typical industrial or laboratory environment they are usually switched on at the beginning of a shift and kept burning until the end of the day. Consequently replacement is needed every 4 to 9 month [12]. In addition, conventional mercury lamps have further drawbacks: machine use of a lithography system with a mercury lamp can only start after about half an hour warm-up time. The bulbs need to be stored and disposed of properly as they contain hazardous mercury. Their handling poses human safety risks and needs to be done by specially trained personnel. Furthermore the supply, use and disposure of mercury lamps will become more difficult and uncertain in a foreseeable future based on the UN Minamata

Convention, the EU Mercury Strategy, the US Mercury Management and other shortly upcoming national and international regulations.
UV-LEDs are a green and safe alternative to mercury lamps. They produce no hazardous waste and there are no human safety concerns. UV-LEDs do not require warm-up times. In addition, LED lamps need much less energy than their Hg counterparts. Figure 7 shows a direct comparison of the energy consumption of a typical MA/BA Gen4 *Pro* mask aligner equipped with a 1 kW Hg-lamp (left) and with an LED source (right). Both offer the same light intensity for exposures. The LED machine requires approximately 60 % less energy during normal operation [12]: the electrical energy consumption is reduced and no exhaust system or special flow cooling is necessary. Some remaining clean dry air and nitrogen volumes are used for wafer processing.

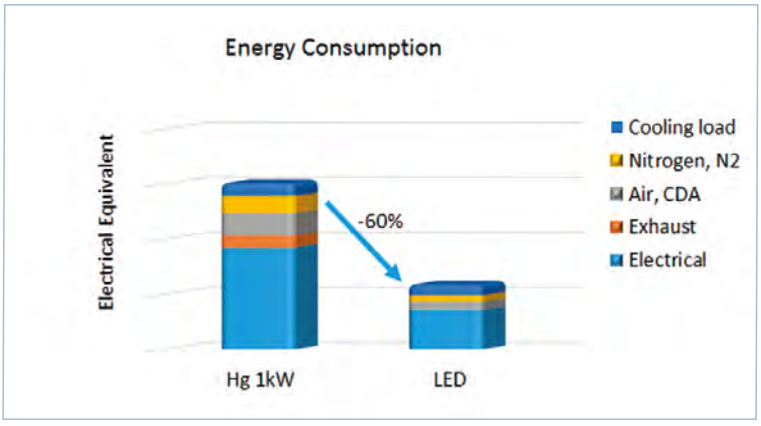

Figure 7 *Energy consumption of a MA/BA Gen4 Pro mask aligner with LED source and equivalent 1 kW Hg- lamp.*

CONCLUSION

We have shown that LED light sources in mask aligners offer strong illumination flexibility by allowing to customize both the intensity and the spectrum of the illumination light. Thus, LED light sources allow optimizing the illumination characteristics for different illumination scenarios and resist materials. We showed that our LED light source has no negative impact on pattern resolution and appearance when compared to a conventional 1 kW Hg-lamp. It offers superior lifetime, reduced power consumption, needs no exhaust system and does not suffer from the disposal problem of conventional Hg-lamps. In combination with SUSS MO Exposure Optics it is now possible to customize the illumination in all three main parameters: wavelength, intensity and illumination angle while at the same time highly homogenous illumination is guaranteed at every point in the mask plane.
In a nutshell the high intensity multi-wavelength UV-LED source is an adequate, green and highly flexible next generation light source for mask aligner lithography.

Acknowledgements

We thank S. Hansen, F. Burgmeier and V. Kolli for their valuable support during measurements and discussions.

References

[1] *Y. Muramoto, M. Kimura, S. Nouda; Development and future of ultraviolet light-emitting diodes: UV-LED will replace the UV lamp; Semicond. Sci. Technol.; vol. 29(8); p. 084004, 2014*

[2] *C. Jeon, E. Gu, M. Dawson; Mask-free photolithographic exposure using a matrix-addressable micropixellated AlInGaN ultraviolet light-emitting diode; Appl. Phys. Lett.; vol. 86; p. 221105, 2005*

[3] *R. M. Guijt, M. C. Breadmore; Maskless photolithography using UV LEDs; Lab on a Chip; vol. 8(8); pp. 1402-1404, 2008*

[4] *S. Suzuki, Y. Matsumoto; Lithography with UV-LED array for curved surface structure; Microsyst Technol; vol. 14; pp. 1291-1297, 2008*

[5] *J. Kim et al.; UV-LED Lithography for 3-D High Aspect Ratio Microstructure Patterning; Proc. Solid-State Sensors and Actuators Workshop Hilton Head; pp. 481-484, 2012*

[6] *Z. Gong et al.; Direct LED writing of submicron resist patterns: Towards the fabrication of individually-addressable InGaN submicron stripe-shaped LED arrays; Nano Research; vol. 7(12); pp. 1849-1860, 2014*

[7] *Y. Li et al.; Rapid fabrication of microfluidic chips based on the simplest LED lithography; Journal of Micromechanics and Microengineering; vol. 25(5); p. 055020, 2015*

[8] *R. Voelkel et al.; "Advanced mask aligner lithography: New illumination system," Opt. Express (to be published)*

[9] *Chu Yih Bing et al.; Microfabrication of surface acoustic wave device using UV LED photolithography technique; Microelectronic Engineering 122; p9-12, 2014*

[10] *Kim et al.; Computer-controlled dynamic mode multidirectional UV lithography for 3D microfabrication; Journal of Micromechanics and Microengineering vol 21.3, p035003, 2011*

[11] *Typical mask aligner resists are strongly sensitive to i-line and less sensitive to h- and g-line light. www.microchemicals.com/de/produkte/fotolacke.html [Aug. 2017]*

[12] *Assuming manual aligner operation for small production with about 12 to 24 wafer exposures per hour during one 8 hour shift per day on 7 days per week, with 1 to 2 sec exposure time*

Dr. Katrin Schindler is Director R&D of proximity lithography equipment at SUSS MicroTec in Garching, Germany.
Katrin graduated in technical physics at the Technical University of Ilmenau, Germany and KTH Stockholm, Sweden. She obtained her doctorate degree in physics on magnetic semiconductor nanostructures at Würzburg University. Before joining SUSS MicroTec in 2010 she worked as application development engineer at ASMLs technology center in Linkou, Taiwan.

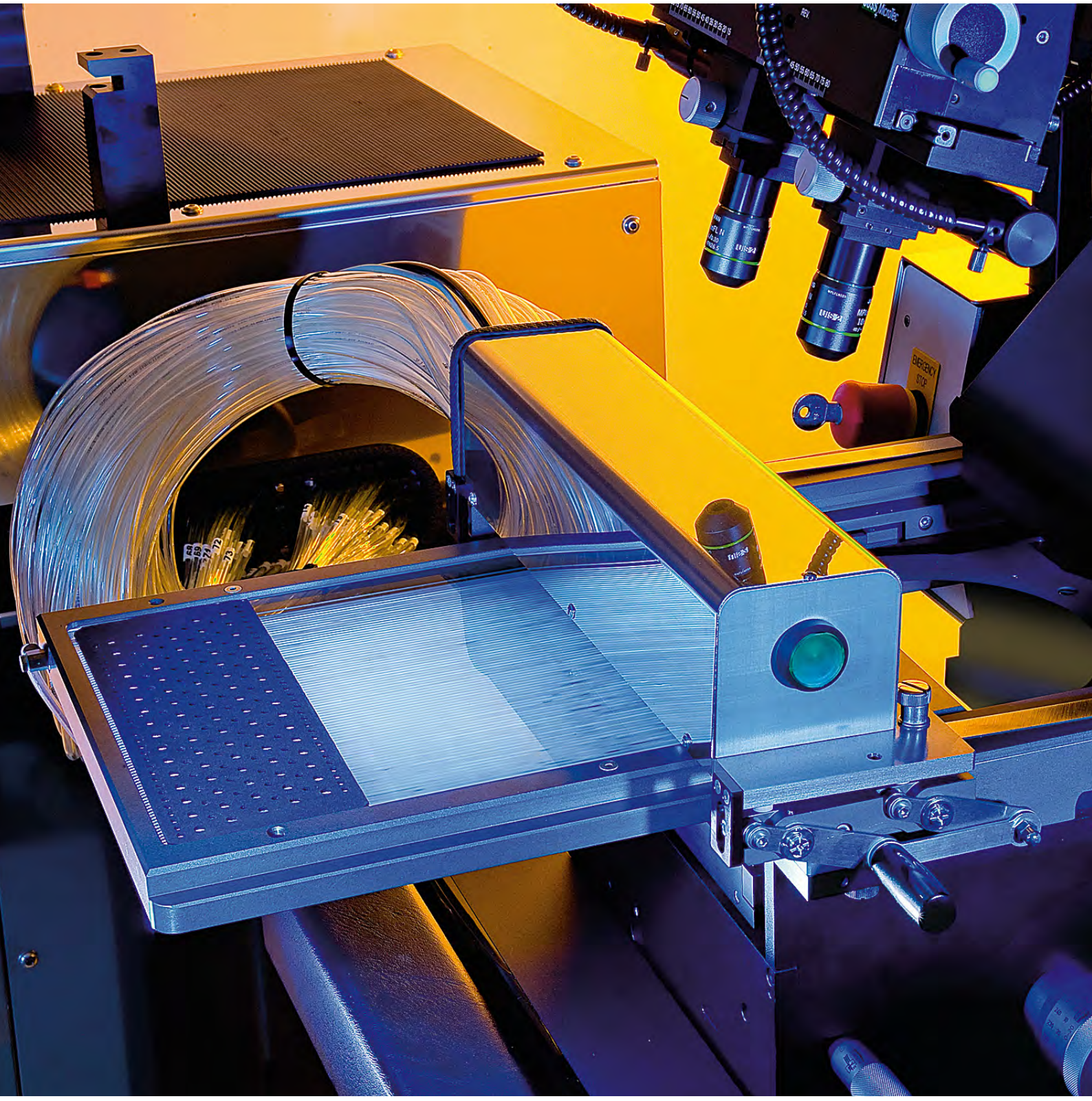
EMERGENCY
STOP

MR-NIL210FC_XP – A VERY PROMISING RESIST FOR EMPLOYMENT OF SCIL TECHNOLOGY IN HIGH VOLUME INDUSTRIAL APPLICATIONS

Michael Förthner Fraunhofer Institute for Integrated Systems and Device Technology IISB, Schottkystraße 10, 91058 Erlangen, Germany
M. Rommel, M. Rumler Fraunhofer Institute for Integrated Systems and Device Technology IISB, Schottkystraße 10, 91058 Erlangen, Germany
M. W. Thesen, M. Messerschmidt, micro resist technology GmbH, Köpenicker Straße 325, 12555 Berlin, Germany
E. Storace SUSS MicroTec Lithography GmbH, Schleissheimerstraße 90, 85748 Garching, Germany

In this work, the performance of the recently developed imprint resist mr-NIL210FC_XP for UV-enhanced substrate conformal imprint lithography (UV-SCIL) from SUSS is evaluated. One major benefit of the material for UV-SCIL is a strongly reduced diffusion behavior of mr-NIL210FC_XP into the PDMS-based SCIL stamps compared to other organic resists. This results in an increased stamp lifetime. A complete imprint process was developed, showing a full wafer pattern transfer while addressing some of the major requirements for production processes, like resist storage time, pattern transfer fidelity and reproducibility, as well as stamp lifetime. The imprinted structures of 50 consecutive imprint processes (including successful automated separation) were found to be highly reproducible, showing height variations well below +/- 2.5 % within individually measured areas. Further tests showed that storage times of at least one week can be applied without any noticeable effect on the imprint result. In order to complete the process chain, the imprinted microstructures were successfully etched into silicon showing homogeneously etched structures.

Nanoimprint lithography (NIL) has been established as a very versatile parallel patterning technique for the fabrication of various functional nanosized features in scientific and industrial devices, e.g. wire grid polarizers, diffractive optical elements, or photonic structures [1, 2]. Over the course of the last years, particularly soft NIL techniques using flexible polydimethylsiloxane (PDMS) stamp materials gained much attention due to their great advantages compared to hard and rigid stamps typically employed in conventional NIL processes [3]. Specifically, soft NIL is very much predestinated for a full wafer patterning of large wafers in one single imprint step [4]. The flexibility of the SCIL stamp leads to a surface conformal imprint ensuring much less sensitivity to particle induced imprint defects because they can be easily overprinted and offers the potential for a patterning of non-planar and other arbitrarily shaped substrate surfaces.

However, the great majority of the currently used soft NIL resist materials suffer from a limited compatibility to PDMS based stamps as resist components like monomers reveal a pronounced propensity to permeate into the PDMS matrix of the stamp. As a consequence of this permeability, the crosslinking of resist components diffused into the PDMS matrix, will result e.g. in the formation of an interpenetrating polymer network at the interface between stamp and resist after several imprints, so that significant tear-off imprint defects during the stamp separation step are very likely to occur. Even before tear-off defects arise, the polymer matrix leads to higher adhesion forces, which can hinder an automated separation. In both cases, the phenomenon significantly reduces the lifetime of a PDMS stamp and thus limits also its utility in a high volume production process. This limitation is particularly relevant when a SCIL working stamp is used for several subsequent imprinting steps, as it would be an essential requirement for an efficient integration of this technology into industrial manufacturing processes [5]. Accordingly, there is a high demand for new soft NIL resists featuring a significantly improved PDMS-stamp compatibility.

In order to address this demand, **micro resist technology GmbH** has developed a new organic photo-curable resist for soft NIL, called mr-NIL210FC_XP. This new NIL resist is a further development of the previously launched mr-NIL210. The mr-NIL210FC_XP formulation contains additional compounds able to effectively suppress the influence of oxygen during the curing reaction, and therefore the cross-linking of the resist components proceeds typically very fast. Hence, imprints can be conducted very readily by applying relatively low illumination intensities in the range of only 10-15 mW cm^{-2} compared to approx. 40 mW cm^{-2} of the predecessor mr-NIL210. Practically, this feature becomes in particular very relevant for the imprinting of resist films with thicknesses significantly below one micrometer, where the impact of the oxygen towards the curing reaction is intrinsically much more pronounced than for thicker films. However, all other resist parameters of mr-NIL210FC_XP are very comparable to those of mr-NIL210 like the outstanding film forming and adhesion characteristics, enabling an extended storage time of spin-coated films over several days without

revealing any negative effects on the film quality. And as the mr-NIL210FC_XP contains only components that feature a very low tendency to permeate into the PDMS matrix of the stamp, imprint defects like adhesion or cohesion failures are very unlikely and adhesion forces are generally reduced, leading thus to a largely prolonged stamp life-time.

The current article details the results of the collaboration project between **Fraunhofer IISB, micro resist technology GmbH,** and **SUSS MicroTec** to fully qualify the new mr-NIL210FC_XP resist within the UV-enhanced substrate conformal imprint lithography (UV-SCIL) from SUSS. The aim was to define and characterize a complete imprint process for an exemplary application, namely etch mask structures usable for patterned sapphire substrate (PSS) fabrication.

For the qualification of the novel UV-NIL resist, all important parameters connected to imprinting were analyzed and partially optimized, like curing time or long-term stability of the uncured resist film, pattern transfer quality, residual layer analysis and stamp lifetime. To define the lifetime of a stamp there exist two different criteria: Firstly, it can be described by the number of imprints before significant stamp degradation would affect feature transfer. It has been previously demonstrated that PDMS stamps could, depending on different parameters, sustain up to several hundred imprints before showing damaging [6]. Secondly, and more pertinently to industrial processes, the definition of stamp lifetime refers to the reached number of automated separations between stamp and imprint before tear-off defects start arising from the imprint process. This latter definition is employed in the current article because automated separation is an essential process step within the applied UV-SCIL technology. Therefore, 50 consecutive imprints were performed with two different stamps without any observable change in separation behavior. Finally, etching experiments were performed to define the etching behavior of this material during reactive ion etching (RIE) into silicon.

SCIL PRINCIPLE AND EQUIPMENT SETUP

Substrate Conformal Imprint Lithography (SCIL) is a NIL technique developed within a collaboration between Philips Research and SUSS MicroTec. It bridges the gap between UV-NIL using rigid stamps for best structure transfer fidelity and soft stamps for imprinting larger substrates with a single imprint step. SUSS mask aligners can be upgraded with SCIL technology, enhancing the aligner's capability by supporting nanoimprint of features with critical dimensions below 50 nm on areas with a diameter of up to 200 mm.

The core blocks of the SCIL principle are (a) the stamp and (b) the imprint procedure. The SCIL stamp is composed of several flexible layers of different blends of PDMS glued to a thin glass carrier. The in-plane stiffness (i.e. the stiffness against lateral distortions) of the thin glass carrier (AF-32, Schott) and the high-modulus X-PDMS (Philips Innovation Services) material of the structured layer minimize lateral distortions during stamp preparation (shrinkage) and imprinting (expansion). The out-of-plane flexibility of the glass carrier and the elasticity of the soft PDMS buffer layer (Sylgard 184) allow the stamp to adapt to the unevenness of the substrate. In addition, the soft PDMS buffer layer provides tolerances to particles between stamp and imprinted substrate.

In order to achieve conformal contact over a large area at low imprint pressure, the SCIL technology uses a process of sequentially bringing stamp and wafer into contact with each other. This sequential contact mechanism prevents from trapping air pockets in between the stamp and the substrate and ensures that the stamp follows the (possibly) uneven topography of the whole substrate surface. For the current project the SCIL tooling was used in combination with a SUSS MA/BA8 Gen4 *Pro* mask aligner.

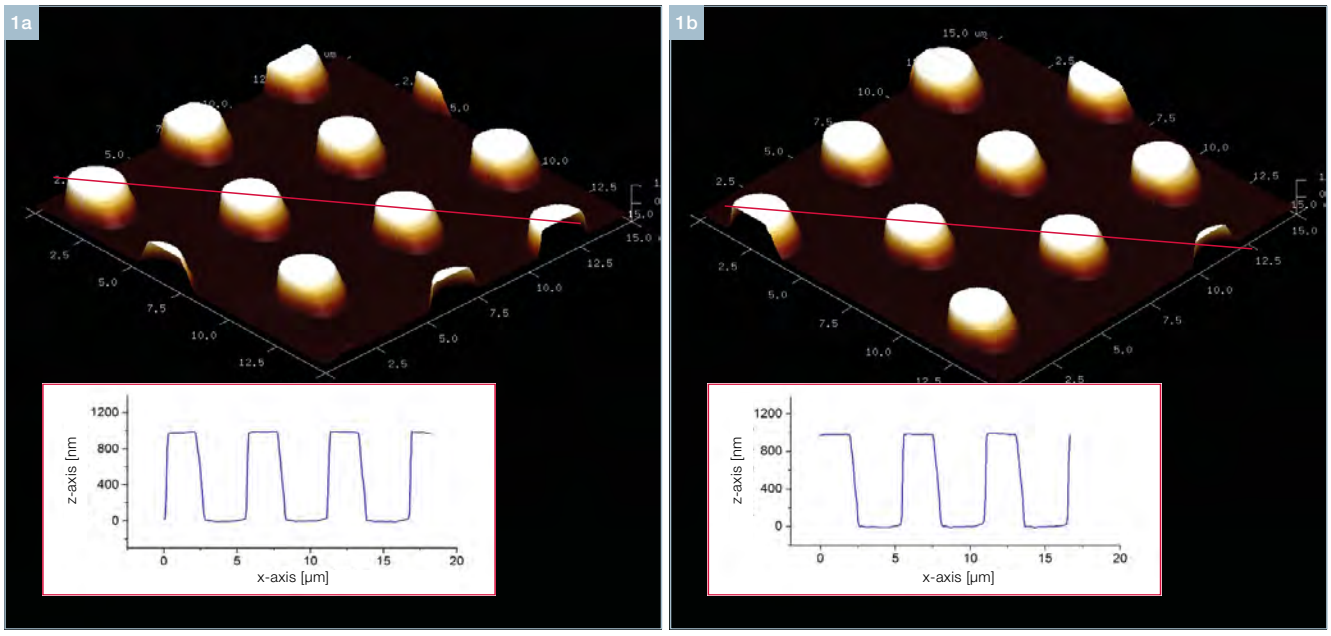

Figure 1 *Images of AFM height measurements of imprinted pillar structures in mr-NIL210FC_XP located (a) between two vacuum groves and (b) below a vacuum grove (imprint parameters are given in the text)*

STAMP MASTER DESIGN AND PREPARATION

The master chosen for the present work was a 150 mm Si wafer containing periodic pillar structures, produced by Fraunhofer IISB via a standard optical lithography process. The dimensions of the pillar structures were the following: pitch 5.6 µm; pillar diameter 2.2 µm. The silicon master showed inhomogeneous etching depths (i.e., pillar heights) ranging from approximately 940 nm to 990 nm (5 % variation over the average pillar height of 965 nm). Since the SCIL working stamp is a one-to-one copy of the master it also showed the same height distribution, which has to be considered when comparing different positions within one imprint or between different imprints. Two identical tri-layered SCIL stamps were produced, one for process demonstration, the second for results validation.

OPTIMIZATION OF PROCESS PARAMETERS AND EVALUATION OF EASE OF RESIST APPLICABILITY

Four imprints were performed using three different exposure times: 30, 60, and 180 seconds. For the setup of this project it was found that after 60 s the structures were fully cured, so that no material re-flow would occur after stamp separation leading to height differences in the imprinted pillars over the whole substrate area (for example, due to the the vacuum groves of the stamp holder [8], as shown in Figure 1, measured by atomic force microscopy (AFM). The average structure height between two vacuum grooves (Figure 1a) was evaluated to be 989 nm +/- 1.4 % and underneath a vacuum groove (Figure 1b) to be 986 nm +/- 1.6 %.

For the investigation of the resist workability over time three wafers were coated with mr-NIL210FC_XP and afterwards soft-baked for 2 min at 90° C. Different storage times before the

Time lag between initial wafer coating and imprint	Simulation of different fabrication procedures	Average pillar height (nm)
10 min	Alignment	959 +/- 2.5 %
1 day	Full-cassette processing	964 +/- 1.3 %
7 days	Shipment between facilities	958 +/- 1.3 %

Table 1 *Average AFM height measurement data of mr-NIL210FC_XP pillars imprinted at different times after initial wafer coating*

imprinting of the coated wafers were applied, to cover and simulate possible cases that can occur in a production environment: The first imprint was performed 10 min after the soft-bake (typical time to perform fully manual alignment), the second imprint 24 hours after the soft-bake (typical time to coat and process a complete cassette of wafers), and the third imprint after 7 days storage time (e.g. for the case that the coated cassette of wafers would be transferred between different facilities or other unexpected production uncertainties). During that time, the wafers were stored in a not-sealed wafer box in cleanroom environment. No difference in resist film quality was observed and, more importantly, also the imprint performance was not affected, even 7 days after the wafers had been initially coated. The resist film remained uniform without any noticeable degradation, material reflow or agglomeration effects. Further on, the quality of the imprinted substrates was within the master specification, as monitored by AFM measurements and summarized in Table 1.

Due to this outstanding film characteristic of the newly developed mr-NIL210FC_XP resist, prepared films facilitate industrial processes as they can be stored after spin-coating over several hours and days.

EVALUATION OF THE IMPRINTING PERFORMANCE OF MR-NIL210FX_XP FOR UV-SCIL

Another main part of the project was to investigate the quality of the structure transfer from the SCIL working stamp to mr-NIL210FC_XP imprint resist. Therefore, five imprints with identical parameters applying the described SCIL working stamp with microsized hole structures were performed on 100 mm Si substrates and for each of them five different positions were analyzed, by scanning electron microscopy (SEM) as well as atomic force microscopy (AFM). Figure 2 shows the high level of uniformity from one of the example cases.

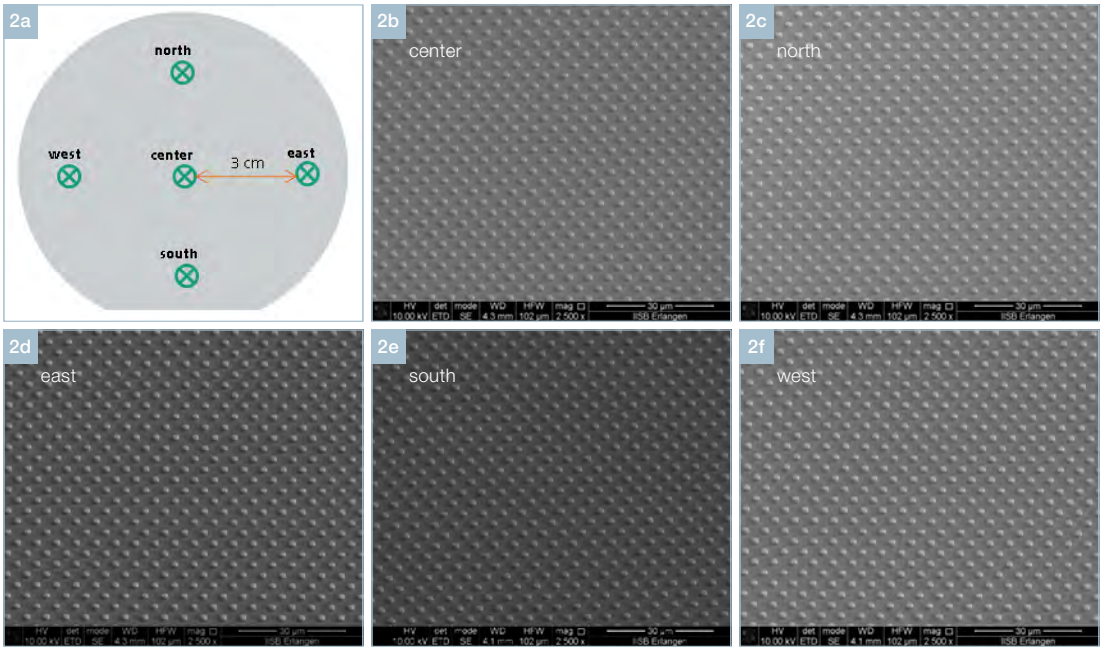

Figure 2 *Illustration of inspected positions for each wafer (a) and corresponding SEM images of imprinted structures at defined positions taken from the first wafer (b-f). Images are tilted by an angle of 52°*

The SEM-images show fully transferred and defect-free qualitative results of the imprinted pillars for every investigated wafer at all inspected positions. AFM measurement results confirm the impression of the SEM images with quantitative data. The structure height does not change systematically for all investigated wafers and positions, laying within the master specifications.

Since a residual layer (RL) value significantly smaller than the feature height is important for further process steps such as etching, RL analysis was performed using SEM investigations at five different positions (see Figure 3). To optimize the final RL thickness, several resist thicknesses have been analyzed via modulating the spin coating recipe and then performing an imprint to measure the resulting RL. By varying the spin speed between 6000 rpm and 6500 rpm, the resist thicknesses (of the soft-baked but not yet UV-cured resist before imprinting) ranged from 170 nm to 180 nm. During the imprint step, the SCIL stamp features will be filled with resist by capillary forces. Within this work, given the height of the master pillars, a RL thickness below 100 nm was targeted and all substrates coated with the spin speeds as mentioned above achieved this requirement. The dependence between the coated layer thickness and the spin speed also showed the potential to achieve even smaller residual layer thicknesses, as the measured RL values decreased within the investigated samples from about 90 nm - 100 nm down to about 50 nm - 60 nm.

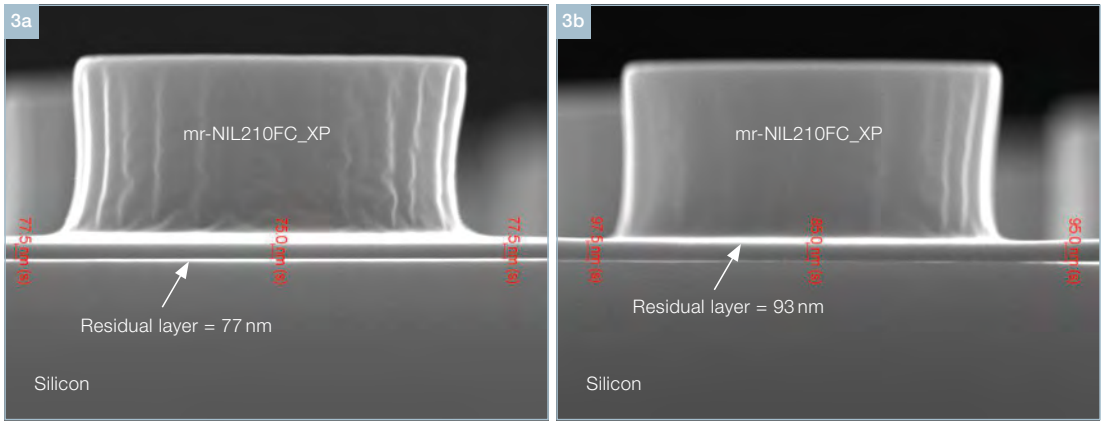

Figure 3 *SEM-images of micro pillars imprinted in mr-NIL210FC_XP. The observed pillar sidewall roughness and shrinkage are considered to derive from the applied 10 kV acceleration voltage during SEM imaging; the left image had a longer observation time than the right one*

INVESTIGATION OF AVERAGE STAMP LIFETIME

As aforementioned for standard SCIL stamps the critical aspect regarding stamp lifetime is typically the automated separation. In order to show the capability of mr-NIL210FC_XP regarding stamp lifetime, 50 consecutive imprints were performed with a first stamp and validated by repeating the tests with a second stamp. In both cases, at least 50 imprints were performed successfully with automated separation, and they all showed a high pattern transfer fidelity. To prove the latter, the first, the twenty-fifth and the fiftieth imprint were analyzed and compared to each other.

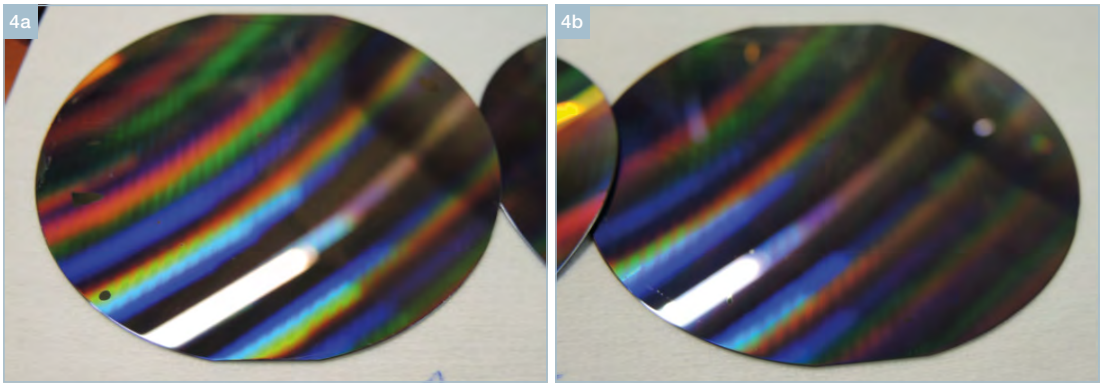

Figure 4 *Photographs of imprint results showing the 1st (a) and the 50th (b) imprint into mr-NIL210FC_XP consecutively processed using one single SCIL stamp*

From the analysis of the results from those imprints, it was clear that more imprints could have still been successfully carried out but an extended stamp lifetime qualification was out of the scope of the present project, and it is planned for follow-up experiments. Figure 4 shows pictures of two imprinted wafers out of the 50 consecutive imprints. The automatic separation of the stamp from the fiftieth imprinted wafer (see Figure 4b) was as easy as for the first one (see Figure 4a). All SCIL specific process parameters (e.g., chuck vacuum) remained unchanged over the course of the imprint study. No yellowing or turbidity or other detrimental effects, as already shown elsewhere with different process conditions [7], were observable on the stamp after the imprints, indicating an extremely low migration of by-products from the curing process from the resist into the PDMS materials. SEM investigations (not shown here) as well as AFM measurements revealed no changes of the dimensions of imprinted patterns (Figure 5).

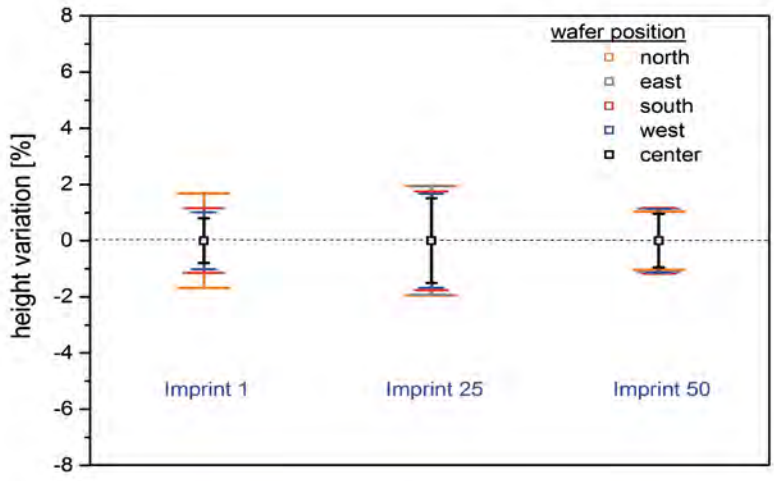

Figure 5 *Average pillar height variation of investigated wafers for lifetime evaluation tests from three different imprints, determined with AFM. The height variation is well below 2 % of the absolute value for each individual imprint (one measurement position covered an area of 15 µm by 15 µm). The total values between different positions are ranging from 890 nm to 950 nm (3 % variation over the average pillar height of 920 nm) with no observable trend with increasing imprint number. These results correspond well to the inhomogeneous etching depth of the master wafer. The small reduction in total height compared to the master of below 4 % can be explained by a common material shrinkage*

ETCHING RESULTS USING HBR RIE PROCESS

As in previous investigations, HBr was chosen for etching of the silicon substrate and Ar-sputtering was employed for removal of the residual layer [8]. All experiments were performed using a Plasmalab 100 system from Oxford Instruments Prior to HBr etching evaluation with mr-NIL210FC_XP, the removal of the residual layer was optimized. Therefore, three samples were treated with 50 sccm Ar at 125 W RF and 800 W ICP power at a chamber pressure of 10 mTorr. The process time was varied between 30 sec, 45 sec, 60 sec and 90 sec. Judging from optical microscope images, the residual layer was apparently removed after 45 sec. Samples were inspected with AFM and SEM to gain depth values of the pillars for each etching experiment.

From standard photolithography applications it is already known that a conducted hard-bake of the patterns before the dry etching for pattern transfer is able to further increase the etching stability of a resist. In order to demonstrate the usability of this approach for UV-NIL, we have performed etching experiments with and without such a hard-bake. After the performed hard-bake of the imprinted structures, no pattern reflow of the pillars was observed, which is a necessary requirement for such an approach. The silicon substrate was structured using 50 sccm HBr at 125 W RF and 800 W ICP power at a chamber pressure of 15 mTorr. Etching experiments without a previously performed hard-bake showed etching rates for mr-NIL210FC_XP of about 90 nm / min. For those samples where an additional hard-bake (100° C, 1 min) was applied the etching rate was below 72 nm / min, leading to an etch selectivity compared to silicon of 1.04 using this particular dry etching recipe applied in our investigations. Etching tests were performed with 2 min and 4 min process time to evaluate the etching rate. A long term etching process (lasting 10 min) resulted in 620 nm deep etched pillar structures with still some remaining resist on top of the pillars. This shows that even higher pillars can be etched using this recipe for longer etching time. The SEM images in Figure 6 show the corresponding etching results. They demonstrate very vertical side walls of the transferred pillars into Si, displaying the excellent usability of the applied UV-NIL resist for RIE etching.

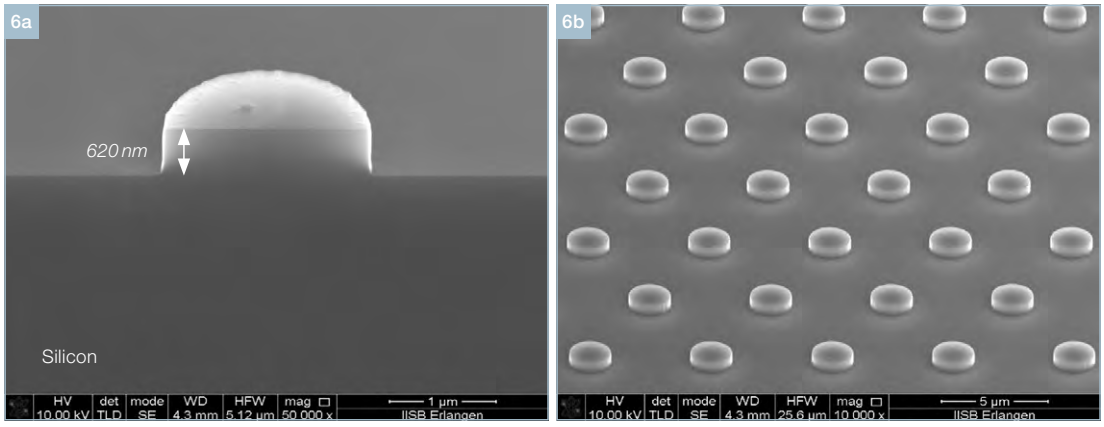

Figure 6 *SEM images after RL removal with Ar sputtering and 10 min HBr etching into silicon. The samples underwent a hard-bake step before etching as discussed above. The left image shows the cross-section of a pillar, where the focal plane is located at the front most part of the feature, to highlight the sharpness of the pillar edges. The roundness of the background portion of the pillar is caused solely by the optical defect from the defocusing. On the right side, an overview to demonstrate the homogeneously etched pillars. Etching depth was 620 nm*

CONCLUSION

A good chemical match between the nanoimprint material and the PDMS stamp is key to enhance stamp lifetime, and, thus, a door opener towards high volume industrial employment of the SCIL technology. The in-depth investigations conducted in the frame of the present work indicate and thus promote the applicability of the UV-SCIL technology in industrial manufacturing processes enabled by the excellent match between the newly developed UV-NIL resist mr-NIL210FC_XP and this particular imprint technology. This success is based on newly implemented resist features, namely excellent film forming and film storage properties, a high imprint fidelity, a fast cross-linking of the resist material due to a very low oxygen sensitivity of the curing reaction when using PDMS stamps, and an excellent pattern transfer fidelity into substrate materials exemplarily shown for silicon and HBr as etch gas in a RIE dry-etch process. Especially of interest for a UV-SCIL application, no influence of the inhomogeneous UV-intensity due to the vacuum groves was found using this UV-resist. Moreover, in the frame of an imprint study with the mr-NIL210FC_XP we could verify that at least 50 consecutive imprints can be conducted with one single SCIL stamp without revealing any indication of a decrease of the imprint quality, indicating that the stamps could have been further employed for many more imprints; an extended stamp lifetime qualification was out of the scope of the present project, and it is planned for follow-up experiments. This highlights that the combination of the UV-SCIL technology with this resist is very suitable for high-volume fabrication processes.

References

[1] *L. J. Guo, J. Phys. D: Appl. Phys. 37 (2004), R123*

[2] *C.-C. Yu, H.-L. Chen, Microelectron. Eng. 132 (2015), 98*

[3] *H. Lan, H. Liu, J. Nanosci. Nanotechnol. 13 (2013), 3145*

[4] *R. Ji, M. Verschuuren, SUSS Report, Vol.2 (2009), 18.*

[5] *I. W. Moran, D. F. Cheng, S. B. Jhaveri, K. R. Carter, Soft Matter 4 (2008) 168.*

[6] *H. Schmitt, P. Duempelmann, R. Fader, M. Rommel, A.J. Bauer, L. Frey, M. Brehm, A. Kraft: Microelectron. Eng. 98 (2012), 275*

[7] *M.J. Haslinger, M.A. Verschuuren, R. van Brakel, J. Danzberger, I. Bergmair, M. Mühlberger: Microelectron. Eng. 153 (2016), 66*

[8] *R. Fader, Substratkonforme Imprintlithographie für optische Anwendungen, PhD Thesis, Erlangen (2014)*

Michael Förthner studied energy engineering at the University in Bayreuth. After graduating in 2012, he continued doctoral research at the Chair of Electron Devices of the University Erlangen in electrical engineering. He is also part of the group for nanopatterning and metrology of the Fraunhofer IISB. Subject of his doctoral thesis is Substrate Conformal Imprint Lithography, especially for the fabrication of Bragg-gratings.

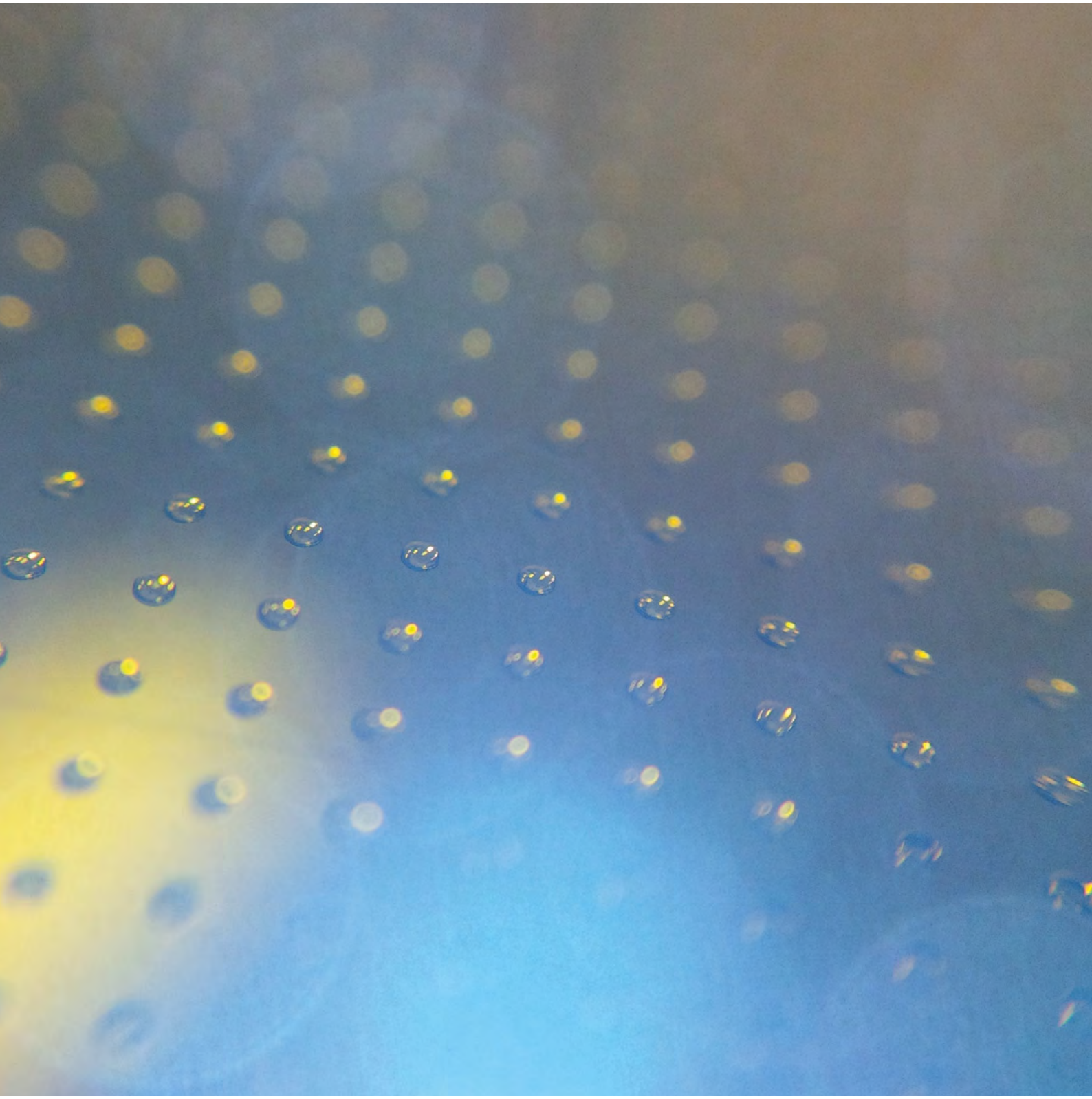

Imprint

Publisher:
SÜSS MicroTec SE
Schleissheimer Str. 90
85748 Garching, Germany
info@suss.com

Register Court Munich
HRB Nr. 235132

Value added
tax identification
number:
DE192123619

Executive Board:
Dr. Franz Richter (CEO)
Robert Leurs (CFO)
Walter Braun (COO)

Chairman:
Dr. Stefan Reineck

Contact:
Hosgör Sarioglu,
Director
Corporate Marketing

NORTH AMERICA

- USA

EUROPE

- Germany
- France
- Switzerland
- United Kingdom

ASIA

- Japan
- China
- Singapore
- Korea
- Taiwan

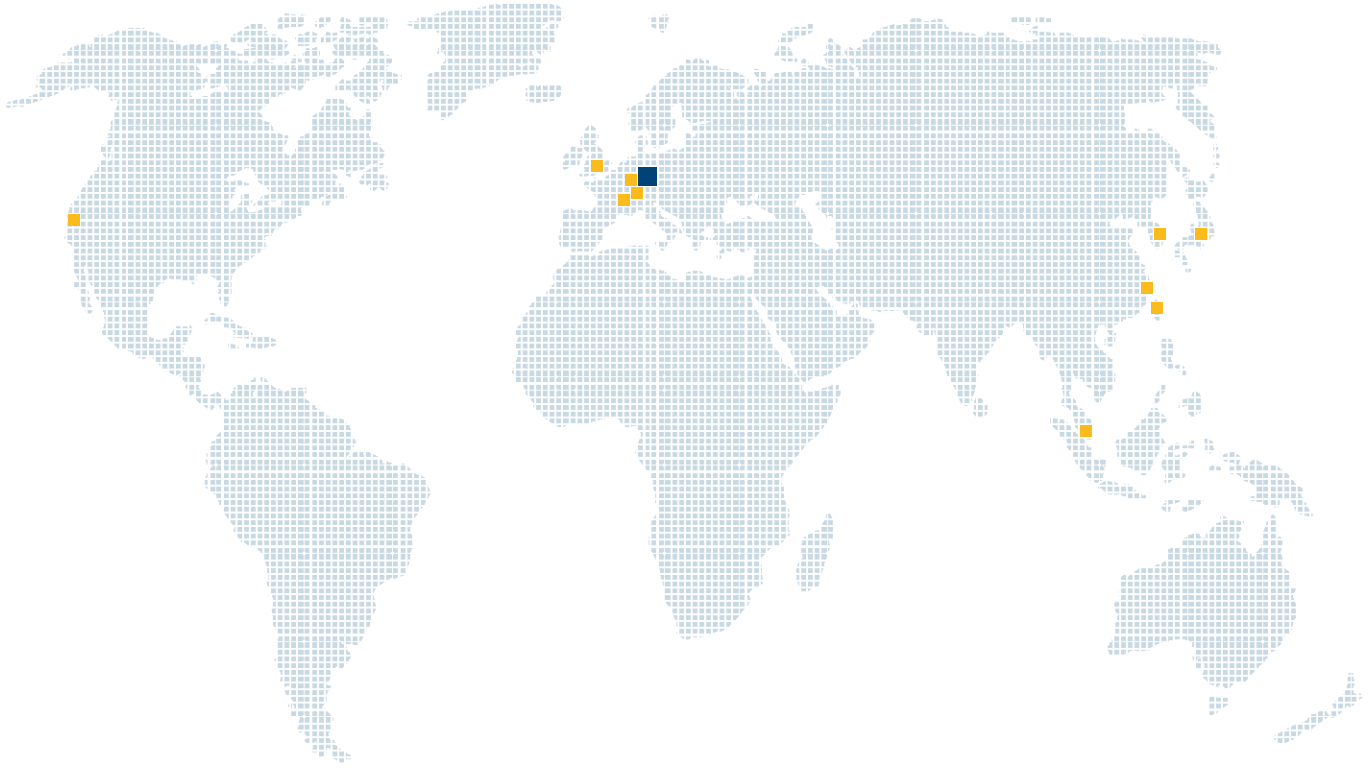

- Headquarters
- Sites

Visit **www.suss.com/locations**
for your nearest SUSS representative or
contact us:
SÜSS MicroTec SE
+49 89 32007-0 · info@suss.com

WWW.SUSS.COM

SÜSS MicroTec